Seasonal variations in the nitrogen isotopic composition of settling particles at station K2 in the western subarctic North Pacific

Yoshihisa Mino・Chiho Sukigara・Makio C. Honda・Hajime Kawakami・Kazuhiko Matsumoto・Masahide Wakita・Minoru Kitamura・Tetsuichi Fujiki・Kosei Sasaoka・Osamu Abe・Jan Kaiser・Toshiro Saino

Y. Mino* ・C. Sukigara

Institute for Space-Earth Environmental Research, Nagoya University, Nagoya, Japan

*e-mail: kuro@hyarc.nagoya-u.ac.jp, Tel: +81-52-789-3491, Fax: +81-52-789-3436

H. Kawakami・M. C. Honda・K. Matsumoto・M. Wakita・M. Kitamura・T. Fujiki・K. Sasaoka・T. Saino

Research and Development Center for Global Change, Japan Agency for Marine-Earth Science and Technology, Yokosuka, Japan

O. Abe

Graduate School of Environmental Studies, Nagoya University, Nagoya, Japan

J. Kaiser

Centre for Ocean and Atmospheric Sciences, School of Environmental Sciences, University of East Anglia, Norwich, UK

Abstract

Intensive observations using hydrographical cruises and moored sediment trap deployments during 2010 and 2012 at station K2 in the North Pacific western subarctic gyre (WSG) revealed seasonal changes in δ^{15}N of both suspended and settling particles. Suspended particles (SUS) were collected from depths between the surface and 200 m; settling particles by drifting traps (DST; 100-200 m) and moored traps (MST; 200 and 500 m). All particles showed higher δ^{15}N values in winter and lower in summer, contrary to the expected by isotopic fractionation during phytoplankton nitrate consumption. We suggest that these observed isotopic patterns are due to ammonium consumption via light-controlled nitrification, which could induce variations in δ^{15}N(SUS) of 0.4-3.1 ‰ in the euphotic zone (EZ). The δ^{15}N(SUS) signature was reflected by δ^{15}N(DST) despite modifications during biogenic transformation from suspended particles in the EZ. δ^{15}N enrichment (average: 3.6 ‰) and the increase in C:N ratio (by 1.6) in settling particles suggests year-round contributions of metabolites from herbivorous zooplankton as well as TEPs produced by diatoms. Accordingly, seasonal δ^{15}N(DST) variations of 2.4-7.0 ‰ showed a significant correlation with primary productivity (PP) at K2. By applying the observed δ^{15}N(DST) vs. PP regression to δ^{15}N(MST) of 1.9-8.0 ‰, we constructed the first annual time-series of PP changes in the WSG. Moreover, the monthly export ratio at 500 m was calculated using both estimated PP and measured organic carbon fluxes. Results suggest a 1.6 to 1.8 times

more efficient transport of photosynthetically-fixed carbon to the intermediate layers occurs in summer/autumn rather than winter/spring.

Keywords nitrogen isotopes; suspended and settling particles; nitrogen recycling; nitrification; primary productivity; export ratio

1. Introduction

The nitrogen isotopic composition of marine organic and inorganic nitrogen species changes depending on their biogeochemical transformations and associated isotopic fractionations (Wada and Hattori 1991). In the euphotic zone (EZ), in particular, the isotope delta of particulate nitrogen, δ^{15}N(PN), is governed by isotopic fractionation during PN formation (i.e. the incomplete utilization of dissolved inorganic nitrogen by phytoplankton). Thus, δ^{15}N(PN) is thought to record nitrogen availability and utilization in the EZ. Negative correlations have been found between δ^{15}N(PN) and the concentration of nitrate (NO_3^-) in the upper mixed layer of several eutrophic regions (Saino and Hattori 1985; Rau et al. 1991; Wu et al. 1997; Altabet et al. 1999; Thunell et al. 2004). Thus, the δ^{15}N of settling particles incorporated into sediments has often been used to reconstruct paleo-nutrient conditions and biological productivity (Calvert et al. 1992; Francois et al. 1992, 1993; Altabet and Francois 1994b; Farrell et al. 1995; Francois et al. 1997; Teranes and Bernasconi 2000; Brunelle et al. 2010).

There are, however, other nitrogen sources for PN formation by phytoplankton, such as ammonium (NH_4^+) and molecular nitrogen (N_2), which have δ^{15}N values that are distinct from preformed NO_3^- (5-7 ‰) supplied from below the euphotic zone (EZ) (Wada and Hattori, 1991). N_2 incorporated by marine nitrogen fixers adds nitrogen with a lower δ^{15}N (-2 to 0 ‰) to the PN pool (Minagawa and Wada, 1984). There are diverging views on the δ^{15}N of the NH_4^+ pool in the upper ocean, which is affected by a variety of processes, including zooplankton excretion, bacterial ammonification,

assimilation by phytoplankton and heterotrophic bacteria, pH, air-sea gas exchange as well as bacterial and archaeal nitrification. Checkley and Miller (1989) reported that NH_4^+ excreted by zooplankton has relatively low $\delta^{15}N$, and as a nitrogen source this NH_4^+ tend to lower the $\delta^{15}N$ of the suspended PN pool (Altabet 1988; Mino et al. 2002). On the other hand, studies by Yoshikawa et al. (2005) and Wankel et al. (2007) suggested that relatively high $\delta^{15}N(NH_4^+)$ values due to preferential ^{14}N consumption by nitrifiers could increase $\delta^{15}N(PN)$ via subsequent assimilation by phytoplankton. The $\delta^{15}N$ of organic nitrogen in the EZ can also be altered during heterotrophic transformations of particles such as metabolism, diagenesis, and trophic transfer in the water column (Saino and Hattori 1980; Minagawa and Wada 1984; Fry, 1988; Aita et al. 2011). Thus, careful consideration is required to unravel the effects of different processes on $\delta^{15}N(PN)$, such as PN formation in the EZ and its transport to the deep ocean, which controls the efficiency of biological pump.

The western subarctic gyre (WSG) of the North Pacific is regarded as an atmospheric CO_2 sink and a more efficient exporter of particulate organic carbon (POC) than other oceanic regions (e.g., Honda et al. 2002; Buesseler et al. 2007; Honda and Watanabe 2010; Kawakami et al. 2014). This is especially true in the early summer when diatoms are dominant (Fujiki et al. 2014; Kawakami et al. 2015), organic carbon produced in the EZ is exported quickly to the ocean interior (Honda et al. 2006). Relative high values of export ratio (*e*-ratio), 46 to 55%, have been found in summer in the WSG (Kawakami and Honda 2007). Honda and Watanabe (2010) highlighted the importance of biogenic opal as “ballast” on vertical POC transport at station K2 in the WSG, in contrast to other

studies which attributed the ballast effect to calcium carbonate (e.g. Francois et al. 2002; Klaas and Archer 2002; Lee et al. 2009). However, knowledge is still scarce on seasonal changes in the efficiency of the biological pump and its controlling factors, which are required for predicting future CO_2 sequestration in the WSG.

The "K2S1 project" described in detail in Honda et al. (Honda et al., this volume) was conducted between 2010 and 2013 to obtain a comprehensive understanding on the seasonal and intra-seasonal variability of ecosystem dynamics and biogeochemical cycles in the western North Pacific. The project involved repeated hydrographical cruises combined with mooring system deployments and satellite data analysis. As part of our studies, we examined δ^{15}N time-series of settling particles collected by a moored sediment trap (MST) at depths of 200 and 500 m at station K2 (47º N, 160º E) in the WSG during 2010 to 2012. In addition, seasonal variations of δ^{15}N for both suspended and settling particles in the upper ocean (0-200 m) were examined during five cruises that were undertaken contemporaneously with the trap deployments and recoveries. These data sets allowed us to investigate: 1) the spatio-temporal variations of δ^{15}N(PN) due to nitrogen recycling and PN formation and 2)the transformation of particles settling in the water column, essential to understand ocean particle dynamics in the WSG. Factors controlling the seasonal variations of primary productivity and *e*-ratio are also discussed based on this data.

2. Materials and Methods

2.1 Collection of settling particles by a moored sediment trap (MST)

Moored sediment trap (MST) time-series experiments were conducted three times during February 2010 to June 2012, in which conical traps were deployed at ca. 200 and 500 m (see Honda et al. this volume), to examine fluxes, chemical composition as well as $\delta^{15}N$ of settling particles. Before deployment, collecting cups were filled with seawater containing 10 % buffered formalin as a preservative. The sampling interval was set to between 6 and 16 days, depending on the planned deployment period of the traps. Following trap recovery, samples were stored in a refrigerator on board until pretreatment (swimmer elimination, splitting, filtration, drying, and pulverization) on shore. The dry weight of trapped particles was measured to estimate total mass fluxes (TMF). Concentrations of organic carbon and nitrogen were measured with a CHN/O elemental analyzer. Those of Al, Si, and Ca were measured with an inductively coupled plasma emission spectrometer. These data were used to estimate the concentrations of organic material, biogenic opal, $CaCO_3$ and lithogenic materials. Full details of sample preparation and chemical analysis have been described elsewhere (e.g. Honda et al. 2002, 2013, this volume). The fluxes of each component were calculated from both TMF and their concentrations in the trapped particles. Subsamples were used to measure the $\delta^{15}N$ of MST particles (section 2.4).

2.2 Collection of suspended particles (SUS) and water samples for $\delta^{15}N$ of nitrate

Samples for $\delta^{15}N$ of suspended particles were collected during five cruises (MR10-06, late October 2010; MR11-02, February to March 2011; MR11-03, April 2011; MR11-05, July 2011; and MR12-02, June 2012) on board R/V *Mirai* (JAMSTEC). 20 to 80 liters

of seawater were collected by CTD/Carousel Water Sampling system with Niskin bottles and a bucket at depths from the surface to 200 m (500 m during MR12-02), and filtered through pre-combusted GF/F filters (Whatman). The filters were kept frozen until analysis on shore. In addition to particle collections, water samples for $\delta^{15}N$ of NO_3^- were also taken during cruise MR10-06. Samples were collected into 50 mL polypropylene bottles at depths between 5 and 1000 m, and then kept frozen until analysis.

2.3 Collection of settling particles by a drifting sediment trap (DST)

During the cruises mentioned above, we conducted short-term, 3 to 4 day-drifting sediment trap (DST) experiments. Cylindrical traps were filled with high-salinity filtrated seawater (S = 39, adjusted by addition of NaCl) and deployed on drifter moorings at approximate depths of 60, 100, 150, and 200 m during all cruises, and at 500 m during MR12-02. More details of these deployments have been described elsewhere (Honda et al. 2015). Particles settled to the bottom of the traps were collected on pre-combusted GF/F filters, and then frozen immediately after swimmers on the filters were removed with tweezers. Concentrations of major components in the DST particles were measured using the methods used for MST particles, as well as $\delta^{15}N$ (section 2.4).

2.4 Isotopic analysis

In the laboratory on shore, finely powdered MST samples and DST and suspended

particles collected on to pre-combusted filters were exposed overnight to HCl fumes to remove carbonates, dried in vacuum, and then pelletized with a tin disk. Mass fractions of particulate organic carbon and nitrogen (POC, PN) and δ^{15}N(PN) in the pellets were measured with an elemental analyzer combined with a continuous flow isotope-ratio mass spectrometer (EA1112-Delta Plus, Thermo Fisher Scientific). The precision for PN and POC mass fractions analysis were better than 3 % and 5 %, respectively. δ^{15}N(PN) values of samples were calibrated against IAEA-N-1. The precision was better than 0.2 ‰, estimated from repeated measurements of laboratory standards (Amino Standard, SI science) along with the samples.. δ^{15}N of NO_3^- was determined using the denitrifier method following Casciotti et al. (2002) and Kaiser et al. (2007), calibrated against IAEA-NO-3. The repeatability was 0.08 ‰, which was derived from the average standard deviation of duplicate analyses.

2.5 Other measurements

Water samples for nutrient and chlorophyll *a* concentrations (Chl *a*) analyses were collected by Niskin bottles during each cruis. Concentrations of NO_3^-, nitrite (NO_2^-) and NH_4^+ were measured on board with a continuous flow analyzer (QuAAtro 2-HR system, BL-Tech). Chl *a* was measured in the particles collected on GF/F filters. Chl *a* on the filters was extracted in N,N-dimethylformamide in the dark at -20 °C for 24 h and then measured in a Turner fluorometer (model 10-AU, Turner Designs), calibrated against a pure chlorophyll *a* (Sigma-Aldrich Co.).

Daily photosynthetic photon flux density (PPFD) and sea surface temperature (SST)

were estimated during the trap deployments from 2010 to 2012 by averaging data acquired by the MODIS satellite over an 11 × 11 pixel square (approximately 100 km × 100 km) centered at station K2. Both estimates were averaged for the sampling interval for MST particles to be analyzed with time-series variations of δ^{15}N(MST).

Results

3.1 Characteristics of particles collected by the moored sediment trap (MST)

This study revealed temporal variations over 2.5 years in particulate organic carbon (POC) flux and the nitrogen isotope delta (δ^{15}N(MST)) of the settling particles collected by sediment traps moored at 200 and 500 m (Fig. 1). For unknown reasons, more than 70 % of trapping cups at 200 m did not collect any particles (Honda et al. this volume). We therefore discuss mainly the characteristics of the settling particles at 500 m.

POC flux averaged over the 2.5-year long deployment was 8.1±8.5 mg m^{-2} d^{-1} (in carbon (C) equivalents) at 500 m. High POC fluxes (>15 mg m^{-2} d^{-1}) were found during May and July to August 2010, July and September to October 2011, and April 2012 (Fig. 1). During these periods, markedly higher fluxes of >30 mg m^{-2} d^{-1} occurred during May 2010 and September to October 2011. Meanwhile, lower values (<5 mg m^{-2} d^{-1}) were found during winter to early spring.

δ^{15}N(MST) at 500 m ranged from 1.9 to 8.0 ‰, with winter maxima and summer minima (Fig. 1). Despite the limited amount of data, values of δ^{15}N(MST) at 200 m (4.0 to 8.3 ‰) were generally consistent with those at 500 m. δ^{15}N(MST) at 500 m was correlated significantly with POC flux (r = -0.50, p <0.001, Table 1, Fig. 2a).

Significant correlations were also found with the organic carbon-to-nitrogen mole ratio (n(C):n(N) ratio, R(C:N); r = -0.67, p <0.001, Table 1 and Fig. 2b). δ^{15}N(MST) was only weakly correlated with the biogenic opal mass fractions, w(opal), and the opal to calcium carbonate mole ratio, R(opal:$CaCO_3$) = n(opal):n($CaCO_3$), of MST particles (r = -0.32 and -0.44, respectively; Table 1). Moreover, significant negative correlations were found with satellite based-daily PPFD as well as SST (r = -0.65 and -0.38, respectively; Table 1). The flux-weighted average δ^{15}N(MST) for the experimental period was 4.1 ‰ at 500 m. This is slightly lower than the δ^{15}N value of NO_3^- (5 to 6 ‰) reported previously for intermediate and deep waters of the Pacific (Tanaka and Saino, 2002; Sigman et al. 2009 etc.).

3.2 Seasonal variation of nitrogen compounds in the water and particles at the upper layer

Five repeat observations between 2010 and 2012 revealed seasonal changes in water density, Chl *a* and nutrients concentrations, δ^{15}N and C:N mole ratio of particles in the upper layer (0-200 m) at K2 (Fig. 3). Mixed layer depth (MLD), determined based on a potential density difference of 0.125 kg m^{-3} from the near-surface (10 m) value (Suga et al. 2004), reached >100 m on February and April 2011 and shoaled to 27 and 39 m on July 2011 and June 2012, respectively (Fig. 3f, k, p, u). The depth of the euphotic zone (EZ), defined as the 0.1 % of surface PPFD level, was around 50 m (39 to 64 m). Depth-average Chl *a* concentrations in the EZ varied from 0.4 g m^{-3} during winter/spring to 1.2 mg m^{-3} in early summer (Fig. 3c, h, m, r, w).

The maximum NO_3^- concentration (25.5 μM) was found in April 2011, associated with the deepest mixed layer (Fig. 3k). During mixed layer shoaling in summer, NO_3^- concentrations decreased as a result of phytoplankton consumption and attained a minimum value of 11.4 μM in late October 2010 (Fig. 3a). As compared to NO_3^-, concentrations of regenerated nutrients, NH_4^+ and nitrite (NO_2^-), showed different seasonal concentration variations. They were found only in the upper 100 m for the entire period, and their concentrations were inversely correlatd to MLD (Fig. 3b, g, l, q, v). In early summer (July 2011, June 2012), distinct NH_4^+ concentration peaks of 1.10 μM were found at the base of the EZ; maximum NO_2^- concentrations of 0.71 μM were found deeper (Fig. 3q, v). It is notable that, during the MR12-02 cruise (June 2012, Fig. 3v), average NH_4^+ concentrations in the EZ increased from 0.35 to 0.65 μM, during a three day-interval between casts. $\delta^{15}N$ of nitrate, $\delta^{15}N(NO_3^-)$ observed in October 2010 during MR10-06 cruise was relatively constant around 5.5 ‰ below the depth of 200 m and increased up to 9 ‰ with decreasing water depth, concomitantly with as nitrate concentrations (Fig.4a), which is attributed to phytoplankton assimilation (e.g. Sigman et al. 1997; Tanaka and Saino 2002).

Concentrations of suspended POC (Fig. 3c, h, m, r, w) were higher in the upper layer and decreased with depth to a nearly constant value (1.1±0.2) μM below 150 m. EZ-averaged concentrations ranged from 2.6 μM in winter to 9.0 μM in summer (Jun 2012), which followed the seasonal variation of chlorophyll *a* concentration. The $\delta^{15}N$ of suspended particulate nitrogen, $\delta^{15}N(SUS)$, exhibited lower values (-0.3 to 3.5 ‰) within the EZ while higher values (3.6 to 10.4 ‰) were found below the EZ (Fig. 3d, i,

n, s, x). Average δ^{15}N(SUS) values weighted by PN concentrations in the EZ exhibited the highest values of 3.1 ‰ in February and the lowest value of 0.4 ‰ in July 2011 (Table 2). The C:N mole ratio of suspended particles, R_{SUS}(C:N), showed a near constant value of around 6 within the EZ during all seasons and increased to between 7 and 10 at greater depths (Fig. 3e, j, o, t, y, Table 2).

Results from DST experiments showed the highest POC flux (75-90 mg m^{-2} d^{-1}) during the productive summer season and lower fluxes (22-27 mg m^{-2} d^{-1}) in winter/spring (Honda et al. 2015). The δ^{15}N value of settling particles collected by DST, δ^{15}N(DST), ranged from 2.1 to 7.4 ‰, and showed distinct seasonal variations (Fig. 1) with little vertical fluctuation from 100 to 200 m (Fig. 3d, i, n, s, x). Depth averagedδ^{15}N(DST) showed the highest values of 7.0 ‰ in February and April 2011 and the lowest value of 2.4 ‰ in June 2012 (Table 2). The C:N mole ratio of DST particles, R_{DST}(C:N), was generally >7.0 (Fig. 3e, j, o, t, y), and the average R_{DST}(C:N) from 100 to 200 m showed the highest value of 9.1 in April 2011 and the lowest of 7.2 in February 2011 (Table 2).

Scatter plots of δ^{15}N against R(C:N) (Fig. 5) indicate obvious differences for the suspended particles in the EZ and the underlying water (100-200 m): the latter had higher values both for δ^{15}N and R(C:N). In addition, a negative correlation (r = -0.76, p = 0.01, n = 11) between them was found for DST particles, except for the MR11-03 cruise (April 2011). This negative correlation was also observed for MST particles at 500 m depth (Fig. 2) and thus particles collected by DST and MST were identical.

DISCUSSION

4.1 Seasonal variation in δ^{15}N of suspended particles and its relation to nitrogen cycle in the mixed layer

The EZ-averaged concentrations of suspended POC at station K2 varied closely with those of Chl *a* resulting in average POC:Chl *a* ratio (*w*/*w*) of 88±13 (n = 6). The typical C:Chl *a* ratio for *in situ* living phytoplankton in the northwestern North Pacific, estimated from both Chl *a* and POC production has been reported as 67 by Obayashi and Tanoue (2002). This suggests that on average 77 % (63 to 92 %) of the POC pool in the EZ is made up of organic matter freshly contributed by autotrophic particles. This observation is also supported by the R_{SUS}(C:N) of around 6 observed in each season (Table 2, Fig. 5), which is close to the Redfield value of 6.6. On the basis of these observations, we can discuss the observed variations of δ^{15}N(SUS) in the EZ with the assumption that it predominantly reflects δ^{15}N of phytoplankton, which in turn is influenced by changes in nitrogenous substrates and their availability for phytoplankton growth.

Previous studies have reported an inverse relationship between δ^{15}N(PN) and nitrate concentrations in the upper layer in various oceanographic regions (Saino and Hattori, 1985; Rau et al., 1991; Altabet and Francois, 1994a), except for oligotrophic regions where N_2 fixation occurs (e.g. Dore et al. 2002). This δ^{15}N behavior has been explained to result mainly from an increase of δ^{15}N of nitrate caused by preferential $^{14}NO_3^-$ uptake during photosynthesis (Miyake and Wada, 1967). However, such a relation was not found in this study (Fig. 7a). The average δ^{15}N(SUS) value within the EZ (0-50 m) varied seasonally by ca. 3 ‰ (Fig. 6c, Table 2): highest (3.1 ‰) and lowest (0.4 ‰)

δ^{15}N values corresponded to higher (1.1 moles m^{-2}) and lower (0.9 moles m^{-2}) nitrate inventories (depth-integrated (0-50 m) nitrate concentration) in winter and in summer, respectively (Fig. 6a).

The vertical profile of δ^{15}N of nitrate observed in October 2010 showed an increase of $\delta^{15}N(NO_3^-)$ with decreasing nitrate concentration, $c(NO_3^-)$ (Fig. 4a). Such an increase of $\delta^{15}N(NO_3^-)$ was attributed to seasonal nitrate consumption by phytoplankton with ^{15}N fractionation, implying that $\delta^{15}N(NO_3^-)$ would be higher and lower during summer/autumn and winter/spring, respectively, in contrast to δ^{15}N(SUS). Applying a Rayleigh fractionation framework, the isotopic fractionation during nitrate removal, $^{15}\varepsilon(NO_3^-)$, can be derived by linear regression of the equation $\delta^{15}N(NO_3^-) = \delta^{15}N(NO_3^-, \text{initial}) + {}^{15}\varepsilon \ln[c(NO_3^-)/c(NO_3^-, \text{initial})]$, where $\delta^{15}N(NO_3^-, \text{initial})$ and $c(NO_3^-,\text{initial})$ correspond to the δ^{15}N and concentration of the initial nitrate pool (we set it as the nitrate found at 100 m), and $\delta^{15}N(NO_3^-)$ and $c(NO_3^-)$ correspond to the profile values. The derived isotopic fractionation is $^{15}\varepsilon(NO_3^-) = -(3.4\pm0.1)$ ‰ (Fig. 4b). Then, using both $\delta^{15}N(NO_3^-)$ and the δ^{15}N of PN synthesized using it, i.e. (δ^{15}N(new PN) = $\delta^{15}N(NO_3^-) + {}^{15}\varepsilon(NO_3^-)$), in the EZ during each cruise were computed (see caption to Fig. 6). The results indicated lower δ^{15}N (6.2 to 6.7 ‰ for $\delta^{15}N(NO_3^-)$; 2.8 to 3.3 ‰ for δ^{15}N(new PN)) result in winter/spring and maxima (9.2 for $\delta^{15}N(NO_3^-)$; 5.8 ‰ for δ^{15}N(new PN)) occur in autumn (Fig. 6a). The δ^{15}N(new PN) computed showed higher values than δ^{15}N(SUS) during any cruise and its variation contradicted the observed variation of δ^{15}N(SUS) (Fig. 6a, c). In all likelihood, this suggested that algal uptake of regenerated nutrients such as NH_4^+, which would add PN with lower δ^{15}N to the

suspended PN pool throughout the year. Alternatively N_2 fixation by diazotrophs can provide for a low $\delta^{15}N$ signal, but the contribution of diazotrophs is most unlikely in the WSG, where seasonal drawdowns of nitrate and phosphate occur with their ratios near the Redfield stoichiometry (ca. 16) and N_2 fixation rate in the surface waters is very low (Shiozaki et al. 2010; Yasunaka et al. 2014).

Shipboard incubation experiments using ^{15}N tracer techniques to access DIN uptake by phytoplankton were conducted during four cruises during 2010 to 2011, which provided an opportunity to deduce seasonal variations of $\delta^{15}N$ of PN formed using NH_4^+ ($\delta^{15}N$(reg. PN)). The results showed that the *f*-ratio (*f*, the fraction of primary production fuelled by NO_3^-) depended on ambient NH_4^+ concentrations ($c(NH_4^+)$) and ranged from 0.4 to 0.8 for $c(NH_4^+)$ <0.4 μM, and from 0.1 to 0.4 for $c(NH_4^+)$ ≥0.4 μM (Matsumoto et al. unpublished data). Here, we compute $\delta^{15}N$(reg. PN) assuming a typical *f*-ratio of 0.6 and 0.3 during winter and summer as well as $\delta^{15}N_{newPN}$ value of 3.3 and 3.9 ‰, and $\delta^{15}N$(SUS) value of 3.1 and 0.4 ‰, respectively (during MR 11-02 and MR11-05 in Fig. 6a,c), and a simple mass balance equation: $\delta^{15}N(SUS) = f\ \delta^{15}N(\text{new PN}) + (1-f)\ \delta^{15}N(\text{reg. PN})$. This computation gives a higher value of $\delta^{15}N$(reg. PN) of 2.8 ‰ in winter and a lower value of -1.1 ‰ in summer, making ca. 4 ‰ difference. This indicates significant seasonal variation of $\delta^{15}N$(reg. PN) as well as its contribution (1-*f*) in controlling $\delta^{15}N$ of bulk PN produced in the EZ (i.e. phytoplankton PN).

Unfortunately, no data exist for this study for $\delta^{15}N$ of NH_4^+ that would affect $\delta^{15}N$(reg. PN). As described above, however, concentrations of regenerated nutrients (NH_4^+ and NO_2^-) showed unique, distinct seasonal changes (Fig. 3b, g, l, q, v). Within the EZ (0-50

m) the NH_4^+ inventory in stratified periods (summer) was about five times higher than in mixing periods (winter/spring) (Fig. 6b). Similarly, the $c(NH_4^+):c(NO_2^-)$ ratio was about four times higher in summer. Such seasonal changes can hint at the behaviors of recycled nitrogen and their $\delta^{15}N$ characteristics (as illustrated in Fig. 8). In general, recycled nitrogen (NH_4^+) in the EZ mainly comes from both bacterial ammonification (Hollibaugh and Azam 1983, Stepanauskas et al. 1999) and zooplankton excretion (Jawed 1973; Hernandez-Leon et al. 2008) (the process iv in Fig. 8). We observed a 1.6-times increase of the NH_4^+ inventory (by 12.3 mmol m^{-2}) within three days during MR12-02 (Fig. 3v and 6b), indicating active production of NH_4^+ occurred within the EZ in summer as reported by Elskens et al. (2008). Interestingly, we also found a concurrent decrease in the Chl *a* inventory by 24.3 mg m^{-2} (Fig. 3w), which assuming an algal C:Chl *a* ratio (*w*/*w*) of 67 and the Redfield C:N mole ratio of 6.6 corresponds to 20.6 mmol m^{-2} (N equivalents). Even though this loss of Chl *a* was rather large relative to the observed increase in the NH_4^+ inventory, these concurrent short-term changes imply that NH_4^+ can be regenerated quickly via decomposition of phytoplankton cells. The $\delta^{15}N$ of NH_4^+ regenerated in the upper oxic water is inferred to be relative low (<-1 %) as a consequence of the kinetic isotope effect during remineralization of organic nitrogen (Macko and Estep 1984; Bada et al. 1989; Checkley and Miller 1989; Silfer et al. 1992; Möbius 2013). Therefore, the reassimilation of such ^{15}N depleted NH_4^+ by phytoplankton has been proposed as the mechanism for lowering the $\delta^{15}N(SUS)$ (Altabet et al. 1988; Mino et al. 2002; Knapp et al. 2011; Treibergs et al. 2014).

On the other hand, NH_4^+ produced in the upper layer was consumed not only by phytoplankton (v in Fig. 8) and heterotrophic bacteria (Kirchman 1994), but also by nitrifying microbes (including ammonium-oxidizing bacteria and archaea) (Ward and Carlucci 1985; Könneke et al. 2005) (vi in Fig. 8). In general, nitrification rate is low in the surface layer and increases to maximum at the base of, or just below the EZ, which contributes the primary nitrite maximum (Ward et al. 1982; Dore and Karl 1996; Ward 2005; Beman et al. 2012; Santoro et al. 2013). Such a decline in nitrification in the EZ has been attributed to the light inhibition (Olson, 1981 etc.) and the competition for NH_4^+ with phytoplankton (Smith et al. 2014: Fripiat et al. 2014). Consequently, photosynthesis is the process responsible for consuming NH_4^+ in the sunlit layer while nitrification takes over in the dimly-lit or aphotic layer where phytoplankton growth is light-limited, as seen in Fig. 8.

It is also possible that nitrification (i.e. NH_4^+ oxidation to NO_2^-) could decrease the $c(NH_4^+)$:$c(NO_2^-)$ ratio effectively. Thus, higher NH_4^+ inventories (20 to 30 mmol m^{-2}) and the high $c(NH_4^+)$:$c(NO_2^-)$ ratio (>2.3) found in summer (Fig. 6b) could result from suppressed nitrification within the bright, upper stratified water, as well as active NH_4^+ production (Fig. 8b). In winter/spring, on the other hand, the competition with phytoplankton for NH_4^+ is reduced (thereby NH_4^+ consumption by nitrifiers was enhanced) by deep mixing across the base of the EZ (Fig. 8a), which would reduce both NH_4^+ inventory and the $c(NH_4^+)$:$c(NO_2^-)$ ratio to the values of 4.4 to 7.9 mmol m^{-2} and 0.6 to 0.8, respectively) as seen in Fig. 6b.

During nitrification, NH_4^+ is subjected to isotopic fractionation of -38 ‰ (Casciotti et al.

2003), which can be larger than that associated with NH_4^+ uptake by phytoplankton (-27 ‰, Waser et al. 1998). Therefore, preferential $^{14}NH_4^+$ oxidation by nitrifiers in the deeply mixed water would cause higher $\delta^{15}N$ of the NH_4^+ pool in winter/spring than that in summer when nitrification was suppressed (Fig. 8). This speculation is consistent with our computed variation of $\delta^{15}N_{regPN}$ with higher (2.8 ‰) and lower (-1.1 ‰) values in winter and summer, respectively. That is, such enriched ^{15}N signal of NH_4^+ via nitrification was imprinted on phytoplankton PN by subsequent photosynthetic uptake (i.e. regenerated production), which would result in the observed higher $\delta^{15}N$(SUS) values in winter/spring relative to summer, as proposed by the numerical models of Yoshikawa et al. (2005) and Shigemitsu et al. (2010a). This is partly supported by the apparent trend of the higher $\delta^{15}N$(SUS) with the lower $c(NH_4^+)$:$c(NO_2^-)$ ratio in the EZ and vice versa (Fig. 7b), given that this ratio indicates the degree of NH_4^+ consumption via nitrification (more contribution by nitrification with lower $c(NH_4^+)$:$c(NO_2^-)$ ratio). Consequently, seasonal variations of NH_4^+ consumption via nitrification, which are controlled by light condition within the upper mixed layer, would determine $\delta^{15}N$(reg. PN) and thereby derive the observed variation of $\delta^{15}N$(SUS) values with higher in winter and lower in summer.

4.2 Formation of sinking particles and their behavior

$\delta^{15}N$ of DST particles, $\delta^{15}N$(DST), exhibited little vertical fluctuation (from 100 to 200 m) while $\delta^{15}N$(SUS) increased with depth in all season (Fig. 3d, i, n, s, x). This was also true for C:N ratios of DST particles (R_{DST}(C:N)) (Fig. 3e, j, t, y) except for data with a

vertical increase found in MR11-03 cruise (Fig. 3o). In this section, we evaluate seasonal variations of $\delta^{15}N_{DST}$ and R_{DST}(C:N) by comparing them with those of suspended particles within the EZ (~50 m) and in the underlying layer (100-200 m) in order to discuss the formation processes of DST particles as well as the behavior of particles during their settling.

δ^{15}N(DST) and R_{DST}(C:N) were always higher than those of suspended particles (mainly contributed by autotrophic particles, i.e. phytoplankton) in the EZ (Fig. 6c, d, Table 2), which implies biological alternation of DST particles during their formation from the photosynthesized organic matters. Such ^{15}N-enrichment in settling particles has been seen in various oceanic areas (Altabet et al. 1988; Wu et al. 1999; Pantoja et al. 2002; Casciotti et al. 2008), which is generally explained by the isotope fractionation associated with the trophic transfer (3 to 4 ‰ per trophic level), leading to higher δ^{15}N of heterotrophs than their dietary nitrogen source (DeNiro and Epstein 1981; Minagawa and Wada 1984; Fry 1988; Aita et al. 2011). As with the body tissue of zooplankton, their fecal material also has a higher δ^{15}N value than the food ingested (Checkley and Entzeroth 1985; Altabet and Small 1990). Observed δ^{15}N difference between the settling particles and phytoplankton (Δ^{15}N(DST-SUS) = (δ^{15}N(DST) - δ^{15}N(SUS)) in this study were 1.4-2.6 ‰ and 3.8-5.4 ‰ in summer and winter/spring, respectively (Table 2). The annual average Δ^{15}N(DST-SUS) of 3.6±1.3 ‰ suggested that DST particles were formed mainly form herbivores if they were produced as a by-product of zooplankton feeding. Zooplankton communities in the western subarctic North Pacific including the station K2 were dominated by herbivorous zooplankton (Taniguchi 1973) such as

copepods *Neocalanus* spp. (Mackas and Tsuda 1999; Kobari et al. 2003; Kobari et al. 2013; Kitamura et al. this volume). In fact, major copepods, such as *Neocalanus cristatus*, *Neocalanus plumchrus*, *Metridia pacifica,* had δ^{15}N values of ca. 5-7 ‰ in MR10-06, MR11-02 and MR11-03 cruises (Kitamura et al., in prep.), which were consistent with δ^{15}N(DST) values obtained in same cruises (Fig. 6c, Table 2). Meanwhile, Honda et al. (2015) reported that opal concentrations in DST particles increased during summer, which indicated that more diatoms contributed to DST particles in summer than in other seasons. This is consistent with the observed decrease of Δ^{15}N(DST-SUS) (i.e. a decline of apparent trophic level of the precursor to DST particles) during July 2011 and June 2012 (in MR11-05 and MR12-02) (Table 2). Consequently, at least with respect to the nitrogen component, the DST particles originated mainly from metabolites (including feces) of herbivorous zooplankton, however contribution of diatoms would increase in summer.

As noted above, R_{DST}(C:N) in MR11-03 cruise showed a vertical increase with higher values of >9 at deeper depth (Fig. 3o). These DST particles collected at 150 and 200 m contained markedly large amounts of lithogenic materials (LM), ca. 13-15 % in concentration, relative to others with averages of 3±2 % (Honda et al. 2015), indicating a significant input of episodic Asian aerosols including dust as well as black carbon etc (Uematsu et al. 1983). Therefore, from here on, we use the R_{DST}(C:N) value of 7.3 at 100 m during MR11-03 as the representative for this term. Average R_{DST}(C:N) from 100 to 200 m showed the lowest value of 7.2 in winter and higher values of 8.1-8.8 in summer whereas C:N of the suspended particles, R_{SUS}(C:N), in the EZ was around 6.0

for all seasons (Fig. 6d, Table 2). Thus, the difference between R_{DST}(C:N) and R_{SUS}(C:N) is larger in summer (Table 2). The C:N mole ratios of zooplankton collected by plankton nets (0.33-mm mesh) during each cruise ranged from 5 to 8 and higher values were observed in summer (Kitamura et al., this volume), which is consistent with R_{DST}(C:N) in summer. On the other hand, zooplankton C:N mole ratios were <5.5 in fall and winter, which alone cannot explain R_{DST}(C:N) of 7.2-7.5 in the same seasons. As an additional source, contributions of transparent exopolymer particles (TEPs) formed from dissolved polymers released by phytoplankton (Alldredge et al, 1993) could raise R_{DST}(C:N). Oceanic TEPs have been known to enhance particle aggregations and their consequent settlement in various environments (Passow et al. 2001; Engel et al. 2004 etc.), which have relatively high C:N mole ratios (>20, Engel and Passow 2001; Mari et al. 2001). Therefore, it is reasonable to assume that contributions of TEPs to the DST particle formation can sustain higher R_{DST}(C:N) than R_{SUS}(C:N) in the EZ, especially given that diatoms that release TEP precursors (Passow et al. 1994) are either the primary or secondary dominant algal group at station K2 all year around (Fujiki et al. 2014). Furthermore, higher R_{DST}(C:N) values during summer could be attributed to increased contributions of organic carbon from TEPs accumulated during a diatom bloom. This enhancement in diatoms is also evident from observations of increased opal concentrations in the DST particles in summer (Honda et al. 2015).

In summary, the higher δ^{15}N and R(C:N) of DST particles as compared to phytoplankton suggests that the organic nitrogen and carbon in DST particles were composed mainly of metabolites (including fecal pellets, Kobari et al. 2013) of

herbivorous zooplanktons such as copepods as well as that of diatoms. Contributions of both diatom cells and TEPs would increase in summer, which is reflected by lower Δ^{15}N(DST-SUS) as well as a further increase in *R*(C:N) in summer than during other seasons. The former strengthens the seasonal δ^{15}N trend (higher values in winter and lower in summer) in the DST particles relative to phytoplankton. The latter provides the trend of higher *R*(C:N) in summer. Both effects would cause the negative relationship between δ^{15}N(DST) and R_{DST}(C:N) as seen in Fig. 2b and 5.

Honda et al. (2015) proposed an annually averaged attenuation of POC flux (via DST particles) in the upper layer at the station K2, in which the settling organic carbon diminishes by 27 % within 100-200 m. On the other hand, only modest changes in δ^{15}N(DST) with depth were found in all season (Fig. 3d, i, n, s, x), which implies the DST particles undergo less remineralization with a diagenetic isotope effect during their settling. Alternatively, the observed attenuation of POC flux (losses of DST particles) would result mainly from the fragmentation of settling aggregates (Karl et al. 1988; Banse 1995; Dilling and Alldredge 2000) as well as the direct grazing by omnivorous zooplankton (Koppemann et al 2004; Steinberg et al. 2008) since both processes had little isotopic effect. Fragmented smaller aggregates with the δ^{15}N value similar to δ^{15}N(DST) were input to the suspended particulate pool, which can partly explain the sharp increases of δ^{15}N(SUS) below the EZ as observed in this study (Fig. 3 d, i, n, s, x). Furthermore it is very likely that the fragmented particles would have been gradually remineralized during longer residence times in the upper layer of 200 m (Goldthwait et al., 2005) relative to the unfragmented DST particles. Consequently, such PN

remineralization with the isotopic effect in the suspended pool might result in higher δ^{15}N(SUS) at 100 to 200 m than δ^{15}N(DST) (annual average 5.6±1.9 ‰ vs. 6.6±0.9 ‰, Table 2). Thus, based on the δ^{15}N properties of both suspended and settling particles at 100 to 200 m, the aggregates in DST particles could break down while settling, which provides a continuous supply of fresh organic material to biota below the EZ.

4.3 Seasonal changes in the productivity and the export ratio at K2

As described above, δ^{15}N(SUS) in the EZ exhibited seasonal variations, which can be attributed to light-controlled nitrification within the mixed layer via the consequent variation in δ^{15}N(reg. PN). It appears that these ^{15}N signatures are imprinted on the DST particles even though they are modulated by ^{15}N enrichments during trophic transfers and the subsequent formation of DST particles. If the δ^{15}N(DST) value varies depending on the photoenvironment of the upper layer, it can serve as an index of primary productivity (PP). By combining δ^{15}N(DST) with the observed PP by ^{13}C tracer method (Matsumoto et al. this volume), we found a significant negative correlation (r^2 = 0.94, Fig. 9a). We then applied this relationship to the time-series δ^{15}N value of MST particles in order to estimate seasonal variations of PP at station K2.

First, the consistency between δ^{15}N(DST) at the depth of 100-200 m and δ^{15}N(MST) at 500 m was confirmed (r^2 = 0.91, n = 4) with a small error in the mean (δ^{15}N(DST) - δ^{15}N(MST)) of +0.3 ‰ (Fig. 9b). After correction for this bias, the RMSE was 0.6 ‰. Second, monthly averages of δ^{15}N(MST) (weighted by PN flux) were calculated from daily data obtained during the entire experimental period from February 2010 to June

2012 (Fig. 10b). Monthly δ^{15}N(MST) values exhibited the maximum value of 7.5 ‰ and the minimum of 2.8 ‰ in February and July, respectively, and correlated negatively with monthly average daily PPFD (r = -0.74) as well as positively with the climatological monthly MLD (r = 0.58; Wakita et al. this volume). These results highlight the cause of δ^{15}N(MST) seasonality; increases correspond to weak insolation and deeper mixing, decreases to strong insolation and stratification, which is similar to observations for both δ^{15}N(SUS) and δ^{15}N(DST). Finally, monthly averaged PP was calculated using the linear regression shown in Fig. 9a, which ranged from 65 to 550 mgC m^{-2} d^{-1} (in carbon equivalents, Fig. 10c). The annual average of calculated PP was 343 mgC m^{-2} d^{-1}, which is very close to the values obtained from seasonal PP observations by ^{13}C tracer technique (315 mgC m^{-2} d^{-1}: Matsumoto et al. this volume).

As depicted in Fig. 10c, PP estimates show higher values in spring/summer (April to August) and lower values in winter (December to March), in accordance with the seasonal trend inferred from changes of underwater optical fields (Honda et al. 2009). Our results are therefore also in agreement with the conclusions from Matsumoto et al. (2014) that light availability exerts a primary control on biological productivity throughout the year. It is somewhat surprising that higher PP occurs during April and May despite the relatively deep MLD of >90 m. This is partly because MLDs in early spring are deeper than the depth of actual “mixing layer” (Brainerd and Gregg 1995), in which the turbulent mixing becomes weak after atmospheric cooling subsides at the end of winter. This situation would increase the residence time of phytoplankton in the EZ thereby alleviating the severe light-limitation that occurs in winter. In addition to light

availability, however, iron availability (Tsuda et al., 2003; Fujiki et al., 2014) and mesozooplankton grazing (Saito et al., 2005) can also influence both the magnitude and duration of diatom blooms, which should be considered in further studies to elucidate the complex mechanisms controlling productivity in the WSG of North Pacific. To understand these complex mechanisms, the availability of seasonal measurements of PP is crucial. Year round PP measurements by traditional shipboard means are scare and methods based on satellite data are limited by heavy cloud and dense sea fog especially in summer (Matsumoto et al. 2014). The approach that we propose, i.e. the use of continuous, time-series δ^{15}N data of MST particles variations of PP can help circumvent the perennial problem of lack of year round PP data

Estimated PP from δ^{15}N(MST) (δ^{15}N based-PP) represents the productivity that occurs when the organic matter in MST particles is formed and thus it can be used as an ideal proxy for calculating export ratio (*e*-ratio), i.e. the ratio of sinking flux of particulate organic carbon to PP. We calculated *e*-ratio from the monthly POC flux at 500 m and estimated PP (Fig. 10d). Monthly averaged POC fluxes showed a clear seasonal variation with higher and lower values in summer and winter, respectively (Fig. 10d), but with relative large standard deviations especially in May, September and October when the two largest peaks of POC flux were found in 2010 and 2011 (Fig. 1). We also calculated *e*-ratios based on average POC flux values for these months, in which case the peak data were excluded (not shown). The calculated *e*-ratio ranged from 0.8 to 4.2 % (Fig. 10d). Its annual average was 2.4 %, which was similar to the value of 2.3 %, albeit on the basis of limited PP data, reported by Honda et al. (Honda et al. this

volume). It has been pointed out that particle fluxes at 500 m are probably underestimates on account of low particle trapping efficiency of the sediment traps (Honda et al. this volume). Based on the average flux of excess ^{210}Pb during 2010 to 2012, Honda and Kawakami et al. (2014) concluded that the trapping efficiency of the MST at 500 m was lower than 100 %. Here we deal with seasonal trends of *e*-ratio without any offset but on the basis of detailed values, although these values are possibly fraught with some degree of uncertainty related with the poor trapping efficiency.

Higher *e*-ratios were found from July to October (2.8-4.2 %) with the maximum in September (Fig. 10d), which was also seen even when two peak data of POC flux were excluded as described above. Meanwhile, lower values (<2.0 %) were found during November to April (or May) with deeper MLD. The minimum value was observed in June although the upper waters had already been stratified. Increase of *e*-ratio by 1.6 to 1.8 times during stratified periods after July suggests that the organic matters produced within the EZ is transported more efficiently to the deep relative to those during well-mixed periods. Actually, *e*-ratio had a negative relation with MLD (r = -0.68, n = 11, Table 3) if the value in June was excluded. Furthermore, *e*-ratio was positively correlated with concentrations of the organic matter fraction (w(OM), %) and R(C:N) for the MST particles with r of 0.67 and 0.71 (n = 12), respectively. These results imply that particle aggregations via TEPs (with higher C:N mole ratio) accumulated in the upper stratified waters and their settling would result in the apparently efficient transport of organic carbon. Conversely, in the deeply mixed water, such aggregates were fragmented (to be suspended particles) due to the turbulent mixing, which would

lower the transport efficiency.

On the other hand, there is no definite relation of *e*-ratio with opal fraction, *w*(opal), (Table 3) which exhibited higher values during March to July (Honda et al. this volume). Seemingly this contradicted with the conclusion in Honda and Watanabe (2010), who reported that biogenic opal plays a crucial role in ballasting of organic carbon to deep sea at K2. However, Honda and Watanabe (2010) also suggested that "the non-ballast associated POC (not transported by ballast minerals such as opal, $CaCO_3$ etc.)" accounted for a relative large fraction (34-82 %) of total POC flux at the depths 150 and 540 m, while it accounted for only 8 % at 4800 m. Therefore we conclude that our estimated *e*-ratio is a more superior reflection of the export efficiency of such non-ballast associated POC to the middle layer (ca. 500 m), which would be governed by the seasonal particle dynamics involving settling aggregate formation in the upper layer. During subsequent settling beyond 500 m (to 4800 m), POC flux to deep sea would be determined significantly by the ballasting role of opal, which would also help to prevent particles from being decomposed by microbes (Honda et al. this volume). This hypothesis however needs further examination, so does the validity of the monthly *e*-ratio estimated here, with more detailed investigations on the particle dynamics in the water column. For instance, the role of particle aggregation via TEP during the stratified period needs to be carefully studied, since the TEP formation and their stickiness can be significantly altered by changes in ocean carbonate chemistry (Mari et al. 2008; Passow 2012), such as decreasing pH in upper mixed waters and shallowing of the calcite saturation horizon (Wakita et al. 2013), which thus has significant consequences for

future biological pump in the WSG.

5. Conclusions

$\delta^{15}N$ of particles trapped at the middle layer (500 m) of the WSG showed higher values in winter when more surface nitrate was available for phytoplankton, and lower values in summer when less nitrate was available. These $\delta^{15}N$ variations reflect mainly seasonal change of surface $\delta^{15}N(NH_4^+)$ due to isotopic fractionation by light-controlled nitrification and subsequent assimilation of ^{15}N-enriched NH_4^+ by phytoplankton. Particle $\delta^{15}N$ values are further modified by biogenic transformations during settling particle's formation. A similar $\delta^{15}N$ pattern of time-series trapped particles has been reported elsewhere in open oceans, the northeastern North Atlantic, subarctic northeastern Pacific and Southern ocean (Voss et al. 1996; Wu et al. 1999; Lourey et al. 2003), where productivity is not limited by macro-nutrients. On the other hand, such $\delta^{15}N$ pattern is contrary to the expected by isotopic fractionation during photosynthetic nitrate consumption, demanding caution when applying $\delta^{15}N(PN)$ as a proxy of surface nitrate utilization. Our observed $\delta^{15}N(PN)$ variations in the WSG were significantly correlated with primary productivity. Interestingly, this negative correlation holds true even in regions where seasonal nitrate depletion occurs, implying that the $\delta^{15}N(PN)$ of sediment trap material can serve as a robust index of productivity over wider oceanographic settings. Furthermore, its application for estimating *e*-ratios with measured organic carbon flux, as conducted here, can be a powerful tool for further understanding of carbon cycles in the modern ocean.

For paleoceanographic purposes, the use of sedimentary δ^{15}N(PN) incorporating seasonal variations, will require careful consideration as to whether nitrification-derived δ^{15}N(PN) enrichment in winter impacts annually integrated δ^{15}N of the settling PN. Based on simulation experiments, Shigemitsu et al. (2010a) suggested that the nitrification isotope effect has only a small influence on the annually integrated δ^{15}N(PN) because the PN flux is low in winter when the nitrification has the largest impact on surface δ^{15}N(PN). Actually, we observed decreases of particle fluxes at 500 m in winter/spring that were attributed to both reduced productivity and low export efficiency. This is because active convective mixing would limit light availability for phytoplankton as well as restrict the physical aggregation of particles. What is important, however, is to what degree the trapped particles would undergo an isotopic alteration during subsequent settling to the sea floor. It is possible that this alteration process is more closely related to seasonal changes of biogenic opal concentrations, because of its influence on the settling velocities of particles and POC remineralization in the WSG (Honda and Watanabe 2010; Shigemitsu et al. 2010b). In conclusion, examination of the validity of annually integrated δ^{15}N(PN) as a measure of the upper-layer nitrogen cycles and its preservation during particle's settling, will require sustained observations of particle dynamics using moored trap at multi-layers (including at near the sea floor).

Acknowledgements

We are grateful to the officers and crew of the R/V *Mirai* for their support during the cruise and to the participants from Marine Works Japan Ltd. for their on-board analysis

and deck works. We also thank Alina Marca, University of East Anglia, for her support of nitrate $\delta^{15}N$ analyses. Thanks to J. I. Goes and H. R. Gomes of Columbia University for their helps to improve this manuscript.

Reference

Aita MN, Tadokoro K, Ogawa NO, Hyodo F, Ishii R, Smith SL, Saino T, Kishi MJ, Saitoh SI, Wada E (2011) Linear relationship between carbon and nitrogen isotope ratios along simple food chains in marine environments. J. Plankton Res 33: 1629-1642.

Alldredge AL, Passow U, Logan BE (1993) The abundance and significance of a class of large, transparent organic particles in the ocean. Deep-Sea Res 40: 1131-1140.

Altabet MA (1988) Variations in nitrogen isotopic composition between sinking and suspended particles: implications for nitrogen cycling and particle transformation in the open ocean. Deep-Sea Res 35: 535-554.

Altabet MA, Small LF (1990) Nitrogen isotopic ratios in fecal pellets produced by marine zooplankton. Geochim. Cosmochim. Acta 54: 155-163.

Altabet MA, Francois R (1994a) Sedimentary nitrogen isotopic ratio as a recorder for surface ocean nitrate utilization. Global Biogeochem Cycles 8: 103-116.

Altabet MA, Francois R (1994b) The use of nitrogen isotopic ratio for reconstruction of past changes in the surface ocean nutrient utilization. In: Zahn R et al. (Eds) Carbon Cycling in the Glacial Ocean: Constrains on the Ocean's Role in Global Change. Springer Verlag, New York, pp. 281-306.

Altabet MA, Pilskaln C, Thunell R, Pride C, Sigman D, Chavez F, Francois R (1999) The nitrogen isotope biogeochemistry of sinking particles from the margin of

the Eastern North Pacific. Deep-Sea Res 46: 655–679.

Bada JL, Schoeninger MJ, Schimmelmann A (1989) Isotopic fractionation during peptide-bond hydrolysis. Geochim. Cosmochim. Acta 53: 3337–3341.

Banse K (1995) Zooplankton-pivotal role in the control of ocean production. ICES J Mar Sci 52: 265-277.

Beman LM, Popp BN. Alford SE (2012) Quantification of ammonia oxidation rates and ammonia-oxidizing archaea and bacteria at high resolution in the Gulf of California and eastern tropical North Pacific Ocean. Limnol Oceanogr 57: 711-726.

Brainerd KE, Gregg MC (1995) Surface mixed and mixing layer depths. Deep-Sea Res I 9: 1521-1543.

Brunelle BG, Sigman DM, Jaccard SL, Keigwin LD, Plessen B, Schettler G, Cook MS, Haug GH (2010) Glacial/interglacial changes in nutrient supply and stratification in the western subarctic North Pacific since the penultimate glacial maximum. Quat Sci Rev 29: 2579-2590.

Buesseler KO, Lamborg CH, Boyd PW, Lam PJ, Trull TW, Bidigare RR, Bishop JKB, Casciotti KL, Dehairs F, Elskens M, Honda MC, Karl DM, Siegel DA, Silver MW, Steinberg DK, Valdes J, Mooy BV, Wilson S (2007) Revisiting carbon flux through the ocean's twilight zone. Science 316: 567-570.

Calvert SE, Nielsen B, Fontugne MR (1992) Evidence from nitrogen isotope ratios for enhanced productivity during formation of eastern Mediterranean Sapropels. Nature 359: 223-225.

Casciotti KL, Sigman DM, Galanter Hastings M, Böhlke JK, Hilkert A (2002) Measurement of the Oxygen Isotopic Composition of Nitrate in Seawater and Freshwater Using the Denitrifier Method. Anal Chem 74: 4905-4912.

Casciotti KL, Sigman DM, Ward BB (2003) Linking diversity and stable isotope fractionation in ammonia-oxidizing bacteria. Geomicrob J 20: 335-353.

Casciotti KL, Trull TW, Glover DM, Davies D (2008) Constraints on nitrogen cycling at the subtropical North Pacific Station ALOHA from isotopic measurements of nitrate and particulate nitrogen. Deep-Sea Res II 55: 1661– 1672.

Checkley DM, Entzeroth LC (1985) Elemental and isotopic fractionation of carbon and nitrogen by marine, planktonic copepods and implications to the marine nitrogen cycle. J. Plankton Res 7: 553-568.

Checkley DM, Miller CA (1989) Nitrogen isotope fractionation by oceanic zooplankton. Deep-Sea Res I 36: 1449– 1456.

DeNiro MJ, Epstein S (1981) Influence of diet on the distribution of nitrogen isotopes in animals, Geochim. Cosmochim. Acta, 45, 341–351, 1981.

Dilling L, Alldredge AL (2000) Fragmentation of marine snow by swimming macrozooplankton: a new process impacting carbon cycling in the sea. Deep-Sea Res I 47: 1227-1245.

Dore JE, Karl DM (1996) Nitrification in the euphotic zone as a source for nitrate, nitrite, and nitrous oxide at Station ALOHA. Limnol Oceanogr 41: 1619-1628.

Dore JE, Brum JR, Tupas LM, Karl DM (2002) Seasonal and interannual variability in sources of nitrogen supporting export in the oligotrophic subtropical North

Pacific Ocean. Limnol Oceanogr 47: 1595-1607.

Elskens M, Brion N, Buesseler K, Van Mooy BAS, Boydc P, Dehairs F, Savoyed N, Baeyens W (2008) Primary, new and export production in the NW Pacific subarctic gyre during the vertigo K2 experiments. Deep-Sea Res II 55: 1594-1604.

Engel A, Passow U (2001) Carbon and nitrogen content of transparent exopolymer particles (TEP) in relation to their Alcian Blue adsorption. Mar Ecol Prog Ser 219: 1-10.

Engel A, Thoms S, Riebesell U, Rochelle-Newall E, Zondervan I (2004) Polysaccharide aggregation as a potential sink of marine dissolved organic carbon. Nature 428: 929-932.

Farrell JW, Pederson TF, Calvert SE, Nielsen B (1995) Glacial-interglacial changes in nutrient utilization in the equatorial Pacific Ocean. Nature 377: 514-517.

Francois R, Altabet MA, Burkle LH (1992) Glacial to interglacial changes in surface nitrate utilization in the Indian sector of the Southern Ocean as recorded by sediment δ^{15}N. Paleoceanography 7: 589-606.

Francois R, Bacon MP, Altabet MA, Labeyrie LD (1993) Glacial/interglacial changes in sediment rain rate in the S.W. Indian sector of Subantarctic waters as recorded by ^{230}Th, ^{231}Pa, U, and δ^{15}N. Paleoceanography 8: 611-630.

Francois F, Altabet MA, Yu E-F, Sigman DM, Bacon MP, Frank M, Bohrmann G, Bareille G, Labeyrie LD (1997) Contribution of Southern Ocean surface-water stratification to low atmospheric CO_2 concentrations during the last glacial

period. Nature 389: 929-935.

Francois R, Honjo S, Krishfield R, Manganini S (2002) Factors controlling the flux of organic carbon to the bathypelagic zone of the ocean. Global Biogeochem Cycles 16(4): 1087. doi:10.1029/2001GB001722.

Fripiat F, Sigman DM, Fawcett SE, Rafter PA, Weigand MA, Tison J-L (2014) New insights into sea ice nitrogen biogeochemical dynamics from the nitrogen isotopes. Global Biogeochem Cycles 28: 115–130.

Fry B (1988) Food web structure on Georges Bank from stable C, N, and S isotopic compositions. Limnol Oceanogr 33: 1182-1190.

Fujiki T, Matsumoto K, Mino Y, Sasaoka K, Wakita M, Kawakami H, Honda MC, Watanabe S, Saino T (2014) Seasonal cycle of phytoplankton community structure and photo-physiological state in the western subarctic gyre of the North Pacific. Limnol Oceanogr 59: 887-900.

Goldthwait SA, Carlson CA, Henderson GK, Alldredge AL (2005) Effects of physical fragmentation on remineralization of marine snow. Mar Ecol Prog Ser 305: 59-65.

Hernandez-Leon S, Fraga C, Ikeda T (2008) A global estimation of mesozooplankton ammonium excretion in the open ocean. J Plankton Res 30: 577-585.

Hollibaugh JT, Azam F (1983) Microbial degradation of dissolved proteins in seawater. Limnol Oceanogr 28: 1104-1116.

Honda MC, Imai K, Nojiri Y, Hoshi F, Sugawara T, Kusakabe M (2002) The biological pump in the northwestern North Pacific based on fluxes and major components

of particulate matter obtained by sediment trap experiments (1997-2000). Deep-Sea Res II 49: 5595-5625.

Honda MC, Kawakami H, Sasaoka K, Watanabe S, Dickey T (2006) Quick transport of primary produced organic carbon to the ocean interior. Geophys Res Lett 33: L16603. doi:10.1029/2006GL026466.

Honda MC, Sasaoka K, Kawakami H, Matsumoto K, Watanabe S, Dickey T (2009) Application of underwater optical data to estimation of primary productivity. Deep-Sea Res I 56: 2281-2292.

Honda MC, Watanabe S (2010) Importance of biogenic opal as ballast of particulate organic carbon (POC) transport and existence of mineral ballast-associated and residual POC in the Western Pacific Subarctic Gyre. Geophys Res Lett 37: L02605. doi:10.1029/2009GL041521.

Honda MC, Kawakami H, Watanabe S, Saino T (2013) Concentration and vertical flux of Fukushima-derived radiocesium in sinking particles from two sites in the Northwestern Pacific Ocean. Biogeosciences 10: 3525-3534.

Honda MC, Kawakami H (2014) Sinking velocity of particulate radiocesium in the northwestern North Pacific. Geophys Res Lett 41: 3959–3965.

Honda MC, Kawakami H, Matsumoto K, Wakita M, Fujiki T, Mino Y, Sukigara C, Kobari T, Uchimiya M, Kaneko R, Saino T (2015) Comparison of sinking particles in the upper 200 m between subarctic station K2 and subtropical station S1 based on drifting sediment trap experiments. J Oceanogr: doi 10.1007/s10872-015-0280-x.

Jawed M (1973) Ammonia excretion by zooplankton and its significance to primary productivity during summer. Mar biol 23: 115-120.

Kaiser J, Hastings M, Houlton B, Röckmann T, Sigman D (2007) Triple oxygen isotope analysis of nitrate using the denitrifier method and thermal decomposition of N_2O. Anal Chem 79: 599-607.

Karl DM, Knauer GA, Martin JH (1988) Downward flux of particulate organic matter in the ocean: a particle decomposition paradox. Nature 332: 438-441.

Kawakami H, Honda MC (2007) Time-series observation of POC fluxes estimated from ^{234}Th in the northwestern North Pacific. Deep-Sea Res I 54: 1071-1090.

Kawakami H, Honda MC, Watanabe S, Saino T. (2014) Time-series observation of 210Po and 210Pb radioactivity in the western North Pacific. J Radioanal Nucl Chem 301: 461-468.

Kawakami H, Honda MC, Matsumoto K, Wakita M, Kitamura M, Fujiki T, Watanabe S (2015) POC fluxes estimated from ^{234}Th in late spring–early summer in the western subarctic North Pacific. J Oceanogr 71: 311-324.

Kirchman DL (1994) The uptake of inorganic nutrients by heterotrophic bacteria. Microb Ecol 28: 255-271.

Klaas C, Archer DE (2002) Association of sinking organic matter with various types of mineral ballast in the deep sea: Implications for the rain ratio. Global Biogeochem Cycles 16: 1116. doi:10.1029/2001GB001765.

Knapp AN, Sigman DM, Lipschultz F, Kustka AB, Capone DG (2011) Interbasin isotopic correspondence between upper-ocean bulk DON and subsurface

nitrate and its implications for marine nitrogen cycling. Global Biogeochem Cycles 25: GB4004. doi:10.1029/2010GB003878.

Kobari T, Shinada A, Tsuda A (2003) Functional roles of interzonal migrating mesozooplankton in the western subarctic Pacific. Prog Oceanogr 57: 279–298.

Kobari T, Kitamura M, Minowa M, Isami H, Akamatsu H, Kawakami H, Matsumoto K, Wakita M, Honda MC (2013) Impacts of the wintertime mesozooplankton community to downward carbon flux in the subarctic and subtropical Pacific Oceans. Deep-Sea Res I 81: 78-88.

Könneke M, Bernhard AE, de la Torre JR, Walker CB, Waterbury JB, Stahl DA (2005) Particulate organic matter and ballast fluxes measured using time-series and settling velocity sediment traps in the northwestern Mediterranean Sea. Nature 437: 543-546.

Koppelmann R., Weikert H, Halsband-Lenk C, Jennerjahn T (2004) Mesozooplankton community respiration and its relation to particle flux in the oligotrophic eastern Mediterranean. Global Biogeochem Cycles 18: GB1038. doi:10.1029/2003GB002121.

Lee C, Peterson ML, Wakeham SG, Armstrong RA, Cochran JK, Miquel JC, Fowler SW, Hirschberg D, Beck A, Xue J (2009) Isolation of an autotrophic ammonia-oxidizing marine archaeon. Deep-Sea Res II 56: 1420–1436.

Lourey MJ, Trull TW, Sigman DM (2003) Sensitivity of $\delta^{15}N$ of nitrate, surface suspended and deep sinking particulate nitrogen to seasonal nitrate depletion in the Southern Ocean. Global Biogeochem Cycles 17(3): 1081. doi:10.1029/

2002GB001973.

Mackas D, Tsuda A (1999) Mesozooplankton in the eastern and western subarctic Pacific: community structure, seasonal life histories, and interannual variability. Prog Oceanogr 43: 335-364.

Macko SA, Estep MLF (1984) Microbial alteration of stable nitrogen and carbon isotopic compositions of organic matter. Org Geochem 6: 787-790.

Mari X, Beauvais S, Lemee R, Pedrotti ML (2001) Non-Redfield C:N ratio of transparent exopolymeric particles in the northwestern Mediterranean Sea. Limnol Oceanogr 46: 1831–1836.

Mari X (2008) Acidification induced upward flux of marine aggregates. Biogeosciences 5: 1631–1654.

Matsumoto K, Honda MC, Sasaoka K, Wakita M, Kawakami H, Watanabe S (2014) Seasonal variability of primary production and phytoplankton biomass in the western Pacific subarctic gyre: Control by light availability within the mixed layer. J Geophys Res Oceans 119: 6523–6534.

Minagawa M, Wada E (1984) Stepwise enrichment of ^{15}N along food chains: Further evidence and the relation between $\delta^{15}N$ and animal age. Geochim Cosmochim Acta 48: 1135–1140.

Mino Y, Saino T, Suzuki K, Maranon E (2002) Isotopic composition of suspended particulate nitrogen ($\delta^{15}N_{sus}$) in surface waters of the Atlantic Ocean from 50°N to 50°S. Global Biogeochem Cycles 16(4): 1059. doi:10.1029/2001GB001635.

Miyake Y, Wada E (1967) The abundance ratio of $^{15}N/^{14}N$ in marine environments. Rec

Oceanogr Works Jpn 9: 37– 53.

Möbius J (2013), Isotope fractionation during nitrogen remineralization (ammonification): Implications for nitrogen isotope biogeochemistry, Geochim Cosmochim Acta 105: 422–432.

Obayashi Y, Tanoue E (2002) Growth and mortality rates of phytoplankton in the northwestern North Pacific estimated by the dilution method and HPLC pigment analysis. J Exp Mar Biol Ecol 280: 33-52.

Olson R (1981) Differential photoinhibition of marine nitrifying bacteria: a possible mechanism for the formation of the primary nitrite maximum. J Mar Res 39: 227-238.

Pantoja S, Repeta DJ, Sachs JP, Sigman DM (2002) Stable isotope constraints on the nitrogen cycle of the Mediterranean Sea water column. Deep-Sea Res I 49: 1609–1621.

Passow U, Alldredge AL Logan BE (1994) The role of particulate carbohydrate exudates in the flocculation of diatom blooms. Deep-Sea Res I 41: 335–357.

Passow U, Shipe RF, Murray A, Pak DK, Brzezinski MA, Alldredge AL (2001) The origin of transparent exopolymer particles (TEP) and their role in the sedimentation of particulate matter. Cont Shelf Res 21: 327-346.

Passow U (2012) The abiotic formation of TEP under different ocean acidification scenarios. Mar Chem 128-129: 72-80.

Rau GH, Sullivan CW, Gordon LI (1991) $\delta^{13}C$ and $\delta^{15}N$ variations in Weddell Sea particulate organic matter. Mar Chem 35: 355-369.

Saino T, Hattori A (1980) ^{15}N natural abundance in oceanic suspended particulate matter. Nature 283: 752-754.

Saino T, Hattori A (1985) Variation of ^{15}N natural abundance of suspended organic matter in shallow oceanic water. In: Sigleo AC, Hattori A (Eds), Marine and Estuarine Geochemistry. A. F. Lewis, New York, pp. 1-13.

Saito H, Suzuki K, Hinuma A, Ota T, Fukami K, Kiyosawa H, Saino T, Tsuda A (2005) Responses of microzooplankton to in situ iron fertilization in the western subarctic Pacific (SEEDS). Prog Oceanogr 64: 223-236.

Santoro AE, Sakamoto CM, Smith JM, Plant JN, Gehman AL, Worden AZ, Johnson KS, Francis CA, Casciotti KL (2013) Measurements of nitrite production in and around the primary nitrite maximum in the central California Current. Biogeosci 10: 7395–7410.

Shigemitsu M, Yamanaka Y, Watanabe YW, Maeda N, Noriki S (2010a) Seasonal characteristics of the nitrogen isotope biogeochemistry of settling particles in the western subarctic Pacific: A model study. Earth Planet Sci Lett 293: 180-190.

Shigemitsu M, Watanabe YW, Yamanaka Y, Kawakami H, Honda MC (2010b) Relationship between sinking organic matter and minerals in the shallow zone of the western subarctic Pacific. J Oceanogr 66: 697-708.

Shiozaki T, Furuya K, Kodama T, Kitajima S, Takeda S, Takemura T, Kanda J (2010) New estimation of N_2 fixation in the western and central Pacific Ocean and its marginal seas, Global Biogeochem Cycles 24: GB1015.

doi:10.1029/2009GB003620.

Sigman DM, Altabet MA, Michener R, McCorkle DC, Fry B, Holmes RM (1997) Natural abundance-level measurement of the nitrogen isotopic composition of oceanic nitrate: An adaptation of the ammonia diffusion method. Mar Chem 57: 227-242.

Sigman DM, DiFiore PJ, Hain MP, Deutsch C, Wang Y, Karl DM, Knapp AN, Lehmann MF, Pantoja S (2009) The dual isotopes of deep nitrate as a constraint on the cycle and budget of oceanic fixed nitrogen. Deep-Sea Res I 56: 1419–1439.

Silfer JA, Engel MH, Macko SA (1992), Kinetic fractionation of stable carbon and nitrogen isotopes during peptide bond hydrolysis: Experimental evidence and geochemical implications. Chem Geol 101: 211–221.

Smith JM, Chavez FP, Francis CA (2014) Ammonium uptake by phytoplankton regulates nitrification in the sunlit ocean. PLoS One 9: e108173.

Steinberg DK, Van Mooy, BAS, Buesseler KO, Boyd PW, Kobari T, Karl DM (2008) Microbial vs. zooplankton control of sinking particle flux in the ocean's twilight zone. Limnol Oceanogr 53: 1327-1338.

Stepanauskas R, Edling H, Tranvik LJ (1999) Differential dissolved organic nitrogen availability and bacterial aminopeptidase activity in limnic and marine waters. Microb Ecol 38: 264-272.

Suga T, Motoki K, Aoki Y, Macdonald AM (2004) The North Pacific climatology of winter mixed layer and mode waters. J Phys Oceanogr, 34: 3–22.

Tanaka T, Saino T (2002) Modified method for the analysis of nitrogen isotopic

composition of oceanic nitrate at low concentration. J Oceanogr 58: 539-546.

Taniguchi A (1973) Phytoplankton-zooplankton relationships in the western Pacific Ocean and adjacent seas. Mar Biol 21: 115-121.

Teranes JL, Bernasconi SM (2000) The record of nitrate utilization and productivity limitation provided by δ^{15}N values in lake organic matter—A study of sediment trap and core sediments from Baldeggersee, Switzerland. Limnol Oceanogr 45: 801–813.

Thunell RC, Sigman DM, Muller-Karger F, Astor Y, Varela R (2004) Nitrogen isotope dynamics of the Cariaco Basin, Venezuela. Global Biogeochem Cycles 18(3): doi:10.1029/2003GB002185.

Treibergs LA, Fawcett SE, Lomas MW, Sigman DM (2014) Nitrogen isotopic response of prokaryotic and eukaryotic phytoplankton to nitrate availability in Sargasso Sea surface waters. Limnol Oceanogr 59: 972–985.

Tsuda A, Takeda S, Saito H, Nishioka J, Nojiri Y, Kubo I, Kiyosawa H, Shiomoto A, Imai K, Ono T, Shimamoto A, Tsumune D, Yoshimura T, Aono T, Hinuma A, Kinugawa M, Suzuki K, Sohrin Y, Noiri Y, Tani H, Deguchi Y, Tsurushima N, Ogawa H, Fukami K, Kuma K, Saino T (2003) A mesoscale iron enrichment in the western subarctic Pacific induces a large centric diatom bloom. Science 300: 958–961.

Uematsu M, Duce RA, Prospero JM, Chen L, Merrill JT, McDonald RL (1983) Transport of mineral aerosol from Asia over the North Pacific Ocean. J Geophys Res 88: 5343–5352.

Voss M, Altabet MA, Bodungen BV (1996) $\delta^{15}N$ in sedimenting particles as indicator of euphotic-zone processes. Deep-Sea Res 43: 33–47.

Wada E, Hattori A (1991) (Eds.), Nitrogen in the Sea: Forms, Abundances, and Rate Processes, CRC Press, Boca Raton, Fla., pp. 208.

Wakita M, Watanabe S, Honda M, Nagano A, Kimoto K, Matsumoto K, Kitamura M, Sasaki K, Kawakami H, Fujiki T, Sasaoka K, Nakano Y, Murata A (2013) Ocean acidification from 1997 to 2011 in the subarctic western North Pacific Ocean, Biogeosciences 10: 7817–7827.

Wankel SD, Kendall C, Pennington JT, Chavez FP, Paytan A (2007) Nitrification in the euphotic zone as evidenced by nitrate dual isotopic composition: observations from Monterey Bay, California. Global Biogeochem Cycles 21: doi:10.1029/2006GB002723GB1081.

Ward BB, Olson RJ, Perry MJ (1982) Microbial nitrification rates in the primary nitrite maximum off southern California. Deep-Sea Res I 29: 247-255.

Ward BB, Carlucci AF (1985) Marine ammonia-oxidizing and nitrite- oxidizing bacteria-serological diversity determined by immunofluorescence in culture and in the environment. Appl Environ Microbiol 50: 194-201.

Ward BB (2005) Temporal variability in nitrification rates and related biogeochemical factors in Monterey Bay, California, USA. Mar Ecol Prog Ser 292: 97-109.

Waser NAD, Harrison PJ, Nielsen B, Calvert HE (1998) Nitrogen isotope fractionation during the uptake and assimilation of nitrate, nitrite, ammonium and urea by a marine diatom. Limnol Oceanogr 43: 215– 224.

Wu J, Calvert SE, Wong CS (1997) Nitrogen isotope variations in the subarctic northeast Pacific: relationships to nitrate utilization and trophic structure. Deep-Sea Res I 44: 287-314.

Wu J, Calvert SE, Wong CS, Whitney FA (1999) Carbon and nitrogen isotopic composition of sedimenting particulate material at Station Papa in the subarctic northeast Pacific. Deep-Sea Res II 46: 2793-2832.

Yasunaka S, Nojiri Y, Nakaoka S, Ono T, Whitney FA, Telszewski M (2014) Mapping of sea surface nutrients in the North Pacific: Basinwide distribution and seasonal to interannual variability. J Geophys Res Oceans 119: doi: 10.1002/2014JC010318.

Yoshikawa C, Yamanaka Y, Nakatsuka T (2005) An ecosystem model including nitrogen isotopes: perspectives on a study of the marine nitrogen cycle. J Oceanogr 61: 921-942.

Legends

Table 1 Results of regression analysis of δ^{15}N(MST) at 500m against data (variables) for fluxes, chemical properties[a] of MST particles and surface environments.

[a]*w*(OC), *w*(opal) indicates mass fraction (%) of organic carbon, biogenic opal, respectively. *R*(opal:$CaCO_3$), *R*(C:N) indicates the mole ratio (*n*/*n*) of opal to calcium carbonate, and organic carbon to nitrogen, respectively.

Table 2 Averaged δ^{15}N and C:N mole ratio (*R*(C:N)) of suspended particles at 0-50 m (SUS, EZ), in the underlying 100-200 m layer (SUS, deep), and in settling particles (DST) collected during each cruise. Δ (DST-SUS, EZ) is the difference of properties between DST particle and SUS particle in the EZ.

[a]*R*(C:N) in brackets represents the values of DST particles at 100 m from MR11-03 cruise when those at the deeper (150 and 200 m) showed relative high *R*(C:N) of >9 and lithogenic contents of >13 %, which was likely due to significant contributions of aeolian dust (see text). [b]Values in brackets were calculated when using *R*(C:N) of DST particles at 100 m as a representative during MR11-03 cruise.

Table 3 Results of regression analysis of monthly E-ratio at 500m against the mixed layer depth (MLD) and chemical properties[a] of MST particles.

[a]*w*(OM), *w*(opal), *w*($CaCO_3$) indicates the mass fraction (%) of organic matter, biogenic opal, calcium carbonate, respectively. *R*(C:N) indicates the organic carbon to nitrogen mole ratio.

Fig. 1 Time series of the particulate organic carbon (POC) flux (bars) and δ^{15}N of the particles collected by moored sediment traps (δ^{15}N(MST); circles) at 200 (white bars/circles) and 500 m (grey bars/circles) depth in the station K2. Also δ^{15}N values of the particles collected by drifting trap (δ^{15}N(DST); black triangles) at 100 to 200 m during five hydrographic cruises are inserted. Cruise ID is shown on top. As for POC flux data, the bar with lower flux between 200 and 500 m was overlaid.

Fig. 2 Relationships of δ^{15}N(MST) at 200 m (white circles) and 500 m (grey circles) with (a) organic carbon flux and with (b) carbon and nitrogen mole ratio, *R*(C:N). The dashed line in Fig. 2b represents a linear fit using reduced major axis (RMA) regression of δ^{15}N(MST) versus *R*(C:N) at 500 m (r^2 = 0.45, n = 55).

Fig. 3 Vertical profiles of parameters in the upper water column observed during five cruises: MR10-06 (a-e), MR11-02 (f-j), MR11-03 (k-o), MR11-05 (p-t), and MR12-02 (u-y). Parameters are sigma theta (σ_θ, top *x*-axis) and nitrate concentrations (NO_3^-, bottom *x*-axis) in the 1st column of panels. Concentrations of nitrite and ammonium ($c(NO_2^-)$, $c(NH_4^+)$) are shown in the 2nd column; chlorophyll *a* (c(Chl, *a*), top *x*-axis) and suspended particulate organic carbon concentrations (c(POC), bottom *x*-axis) in the 3rd column; δ^{15}N of suspended (SUS) and settling (DST) particles in the 4th column; organic carbon to nitrogen mole ratio (*R*(C:N)) of particles in 5th column. Different profiles of $c(NO_2^-)$ and $c(NH_4^+)$ (panel v), c(Chl *a*) (panel w) during MR12-02

correspond to the data collected during earlier and later period of observation, which stresses short-term (<3 days) changes in these parameters. Horizontal solid and dotted lines indicate mixed layer depth (MLD) and the depth of euphotic zone (ELD), respectively.

Fig. 4 (a) Vertical profiles of both nitrate concentration ($c(NO_3^-)$) and $\delta^{15}N$ of nitrate at the station K2 in October 2010 (during MR10-06). (b) Nitrate $\delta^{15}N$ vs $\ln[c(NO_3^-)]$ for the profile data in Fig. 4a. Dashed line represent a linear fit to the data in the upper 100 m ($r^2 = 0.997$, $n = 7$ $p < 0.001$), which gives a slope of –3.4±0.1 ‰ corresponding to the isotope effect ($^{15}\varepsilon(NO_3^-)$) for nitrate consumption by phytoplankton following the Rayleigh fractionation model (see text).

Fig. 5 Relationship between R(C:N) and $\delta^{15}N$ of both suspended and settling particles. Open and grey squares denote suspended particles within the euphotic zone (SUS, EZ) and from the underlying depth from 100 to 200 m (SUS, deep), respectively. Black triangles denote the settling particles collected by the drifting sediment traps (DST) at the depth from 100 to 200 m. Data for DST particles collected during MR11-03 are represented as open triangles. Dashed line represents a linear fit using RMA regression between $\delta^{15}N$ and R(C:N) of MST particles at 500 m seen in Fig. 2b. The properties of DST particles follow the same trend, except for those from MR11-03.

Fig. 6 Temporal changes in (a) depth-integrated (0-50 m) nitrate inventory (grey bars)

and modeled $\delta^{15}N$ of nitrate ($\delta^{15}N(NO_3^-)$, closed circles) and PN formed from it ($\delta^{15}N$(new PN), closed squares) in the EZ. (b) depth-integrated ammonium and nitrite inventories (black and white bars, respectively) and their ratios (white circles). Averaged (c) $\delta^{15}N$, (d) *R*(C:N) of suspended particulate pool in the EZ (SUS, EZ; white squares) and the lower layer (100-200 m) (SUS, deep; grey squares) and settling particles (DST, black triangles) at 100-200 m. The error bars denote the standard error of the mean. Note: NO_3^-, NO_2^- and NH_4^+ inventories during MR12-02 cruise in Fig. 6a and 6b have different symbols for the earlier and later part of the cruise, as seen in Fig. 3v. The time-evolution of $\delta^{15}N(NO_3^-)$ and $\delta^{15}N$(new PN) in Fig. 6a was estimated by a simple Rayleigh fractionation model assuming nitrate was consumed seasonally with $^{15}\varepsilon(NO_3^-)$ of -3.4 ‰ and using the observed ratio of surface to deeper (100 m) nitrate concentrations and $\delta^{15}N(NO_3^-$, initial) of 5.9 ‰ found at 100 m (see Fig. 4b and text).

Fig. 7 The relation of average $\delta^{15}N$ of suspended particles in the EZ versus (a) the NO_3^- inventory and (b) the ratio of NH_4^+ to NO_2^- concentrations in the upper layer of 50 m. The solid line indicates a linear regression between variables (r = -0.64, p = 0.24).

Fig. 8 Simplified nitrogen cycling in the upper water column during (a) winter and (b) summer at the station K2. Arrows indicate fluxes: (i) NO_3^- transport due to winter convection, (ii) NO_3^- uptake by phytoplankton, (iii) PN sinking, (iv) Regeneration of NH_4^+ (ammonification by heterotrophs), (v) NH_4^+ uptake by phytoplankton, (vi) NH_4^+ oxidation by nitrifiers, (vii) NO_3^- diffusion. Dotted and dashed lines indicate depths of

the euphotic layer (ELD) and the mixed layer (MLD), respectively. For fluxes (v) and (vi), the isotopic fractionations associated with them are described as ε_{ntrA} and ε_A, respectively. All nitrogen within the mixed layer ultimately originates from deep water NO_3^- supplied by wintertime vertical mixing (i). This preformed nitrate is consumed by phytoplankton (ii) to form particulate nitrogen. Part of PN is removed as sinking PN from the mixed layer (iii). Another part is remineralized to ammonium by microbial ammonification (iv). Ammonium can then be reassimilated into the PN pool by algal uptake in the euphotic layer (v) or oxidized by nitrifiers to nitrite (vi), and further oxidized to nitrate in the aphotic layer. Here we assume that NH_4^+ oxidation by nitrifiers in the euphotic layer is suppressed due to the light inhibition and the competition with phytoplankton (see text). The balance of these fluxes and the isotopic fractionations associated with them determine the $\delta^{15}N$ of each nitrogen pool.

As for the ammonium pool in summer (Fig. 8b), it is regulated by both regeneration (iv) and re-assimilation (v) of NH_4^+ in the shallow mixed layer. Below the euphotic layer, NH_4^+ oxidation (vi) occurs but does not affect the ammonium pool within the upper mixed layer (and the euphotic layer). On the other hand, in winter (Fig. 8a) nitrification does affect the ammonium pool since the MLD is deeper than the ELD. The isotopic fractionation during ammonium oxidation (ε_{ntrA}) is larger in magnitude than the isotopic fractionation during assimilation (ε_A). This can make the residual ammonium pool more enriched in ^{15}N in winter relative to that in summer.

Fig. 9 (a) Correlation between the averaged $\delta^{15}N$ value of DST particles ($\delta^{15}N$(DST)) at

100 to 200 m depth and the primary productivity measured during each cruise (Matsumoto et al. 2014). The solid line indicates a linear regression between them (r^2 = 0.94, p = 0.007). (b) Comparisons of averaged δ^{15}N(DST) with δ^{15}N of MST particles (δ^{15}N(MST)) at 200 and 500 m (open and closed circles, respectively). Data were used for both particles collected around the same period. The dotted line represents a 1:1 relationship. δ^{15}N(MST) at 500 m correspond toδ^{15}N(DST) with the mean error of 0.3 ‰, albeit the data limited (n = 4).

Fig. 10 Monthly variations in (a) daily PPFD (diamonds)[a], (b) climatological mixed layer depth (MLD, white squares) and δ^{15}N of the MST particles (δ^{15}N(MST), black circles) at 500m depth, (c) primary productivity (PP, bars)[b] estimated from δ^{15}N(MST), (d) particulate organic carbon (POC) flux (bars)[c] and the export ratio (e-ratio = POC flux/PP, circles[d]) at 500m. Notes: [a]Data were acquired by the MODIS satellite. [b]Productivity was estimated by applying the δ^{15}N vs. PP regression (Fig. 9a) to monthly δ^{15}N(MST) data. [c]Monthly average of POC flux was calculated from daily data obtained on the assumption that it was same during respective sampling periods. [d]Black circles represent the E-ratio in the case two peaks of POC flux found in May 2010 and September/October 2011 (Fig. 1) were excluded in the calculation for monthly values. Dashed lines in Fig. 10d indicate the averaged e-ratio of 2.0 and 3.4 % during mixed (Nov. to May.) and stratified (Jul. to Oct.) periods, respectively.

Figure 1 (Mino et al.)

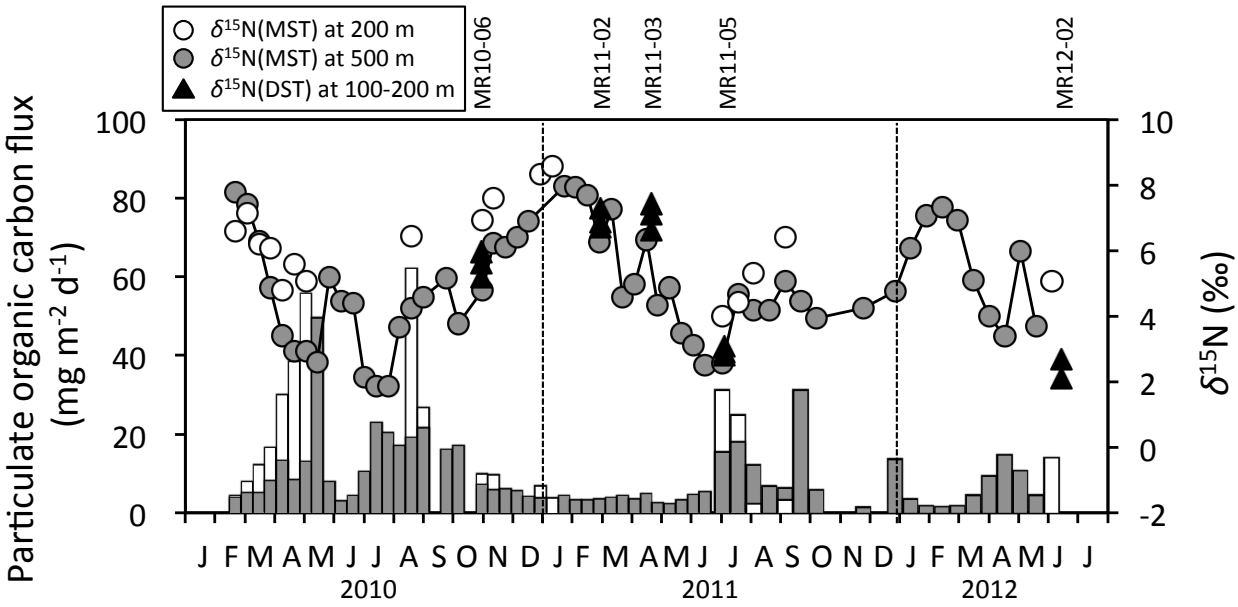

Figure 2 (Mino et al.)

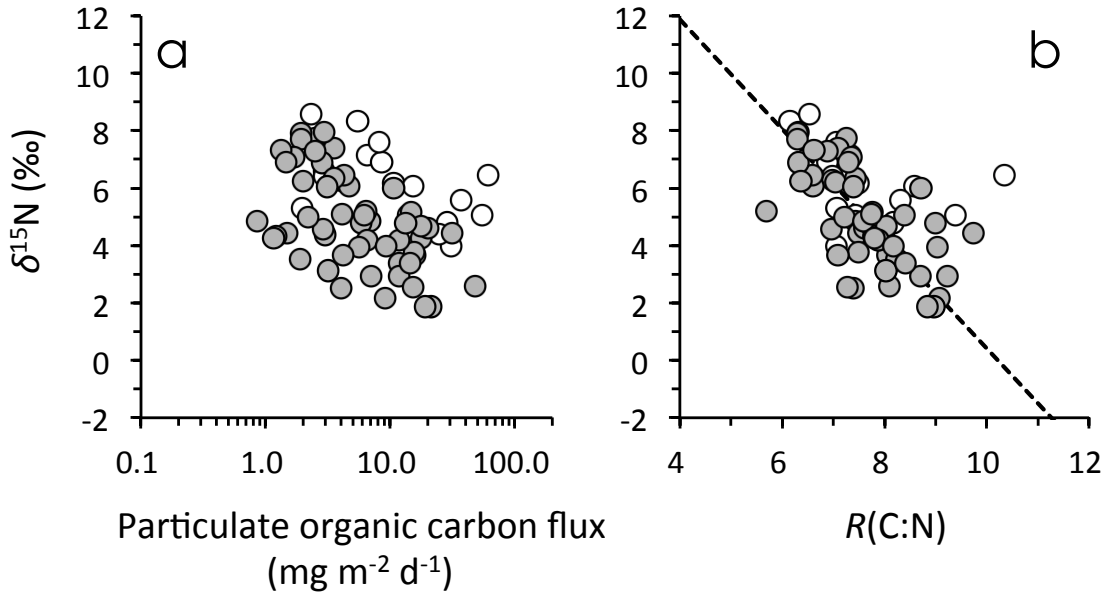

Figure 3
(Mino et al.)

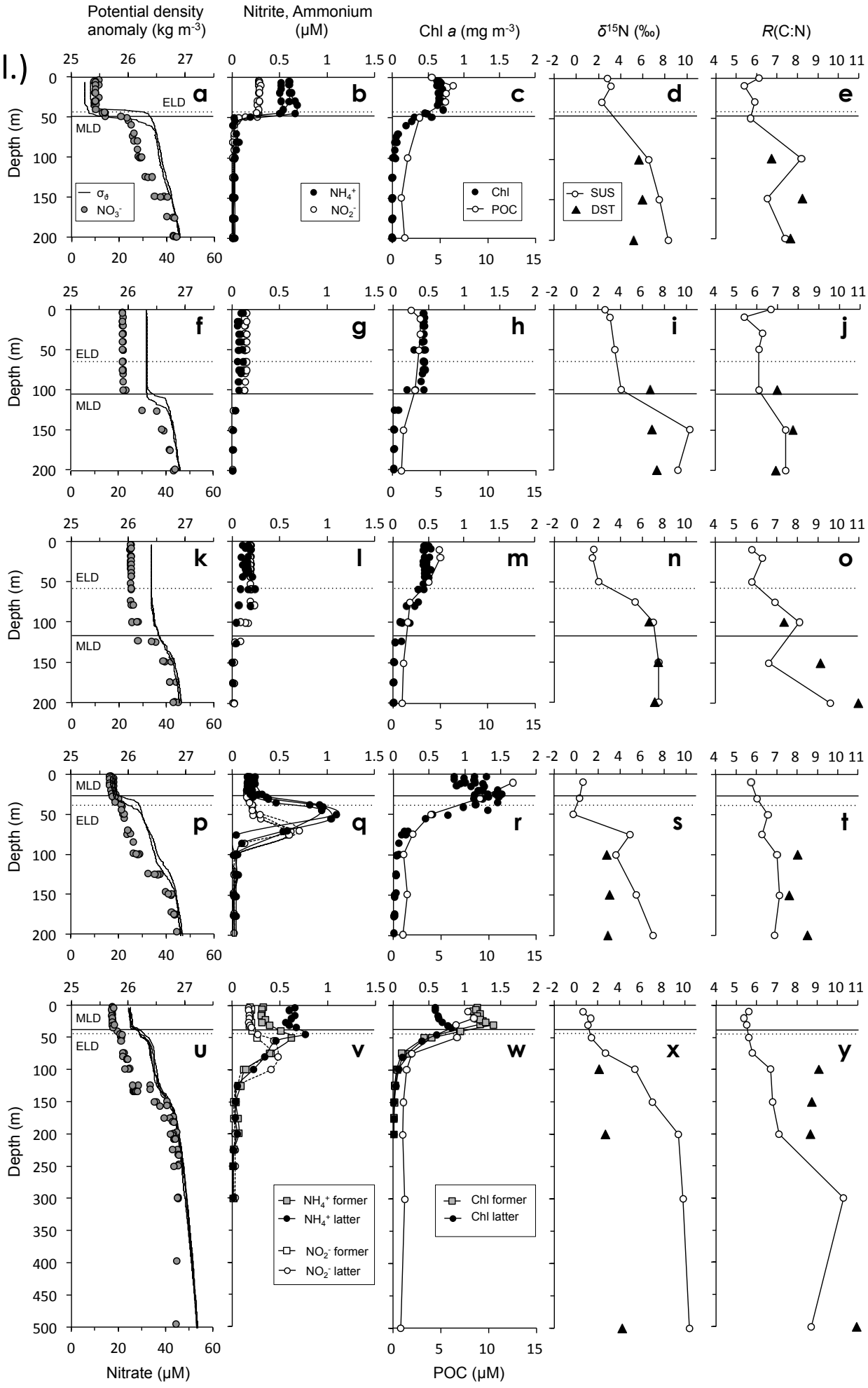

Figure 4 (Mino et al.)

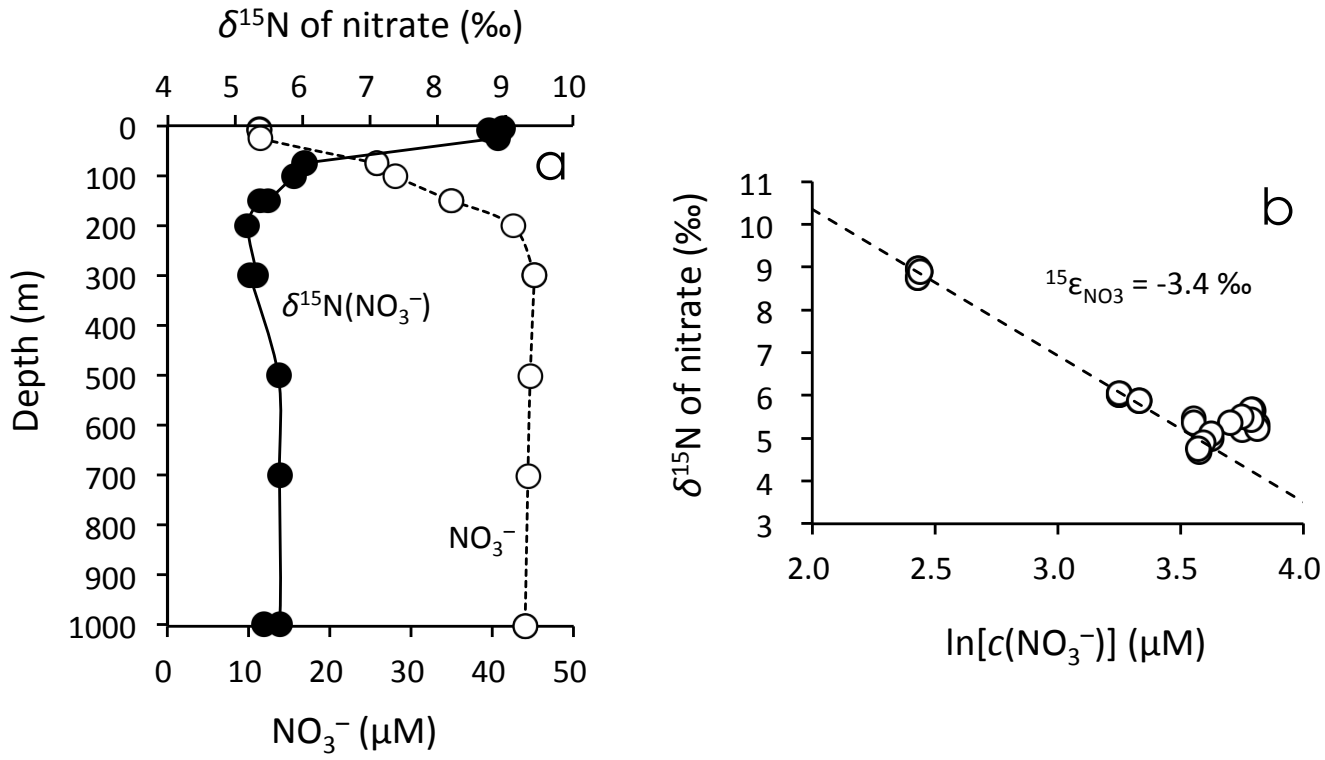

Figure 5 (Mino et al.)

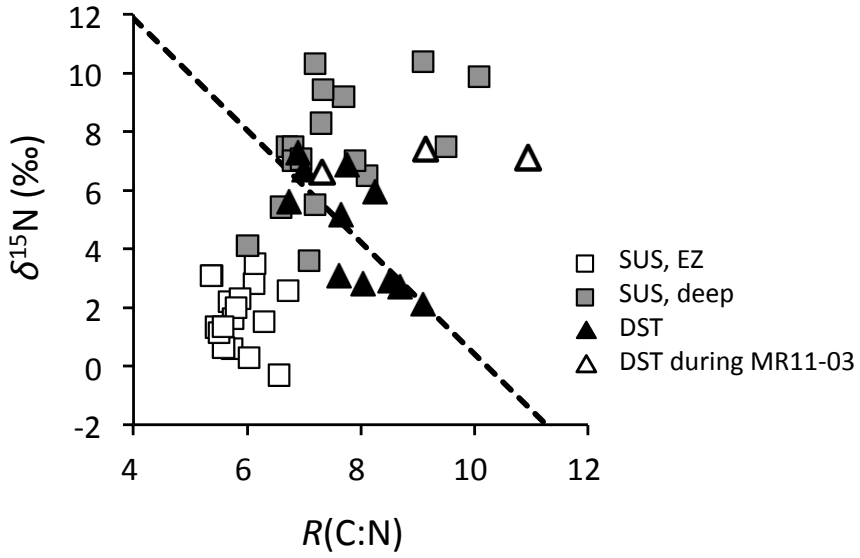

Figure 6 (Mino et al.)

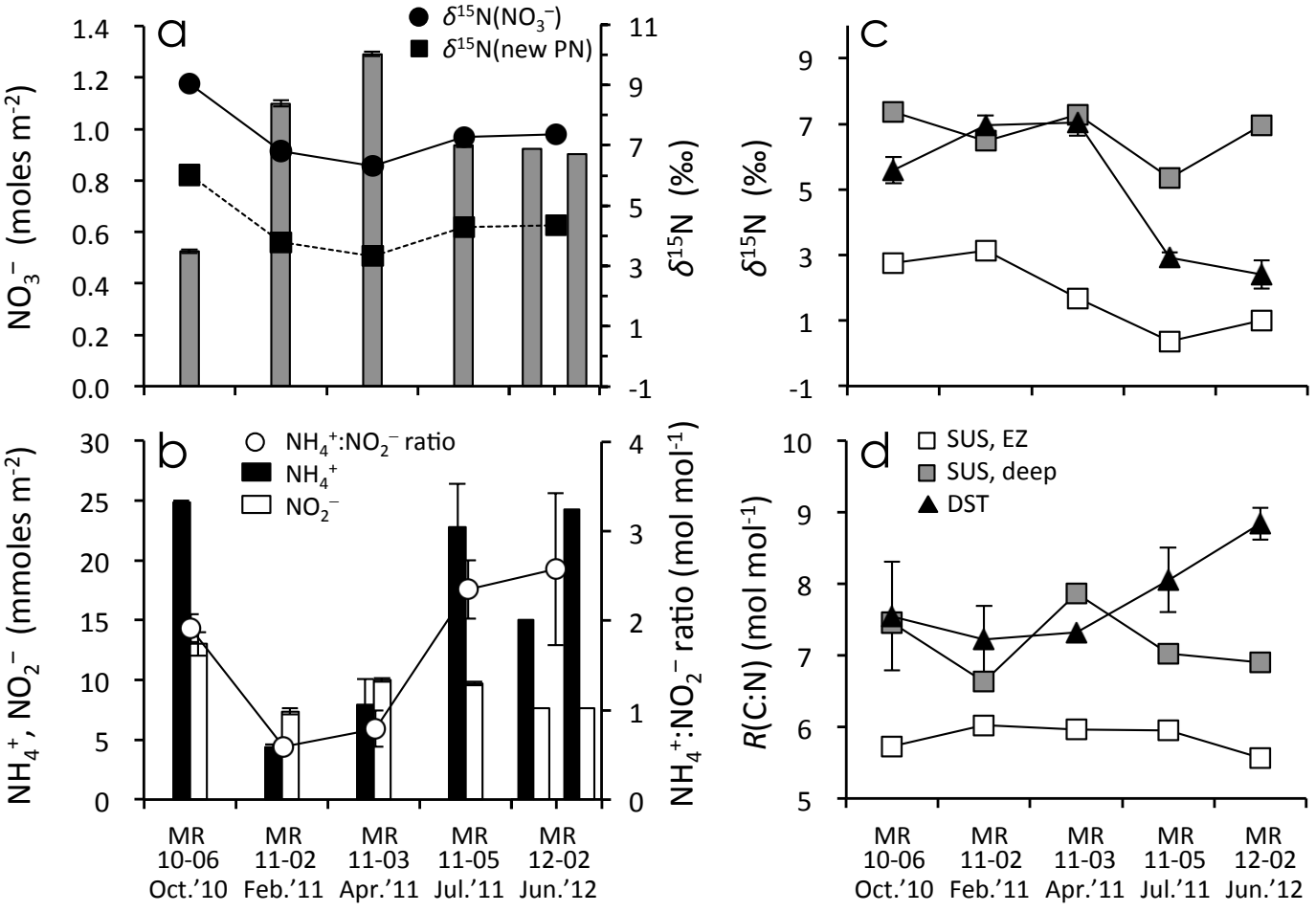

Figure 7 (Mino et al.)

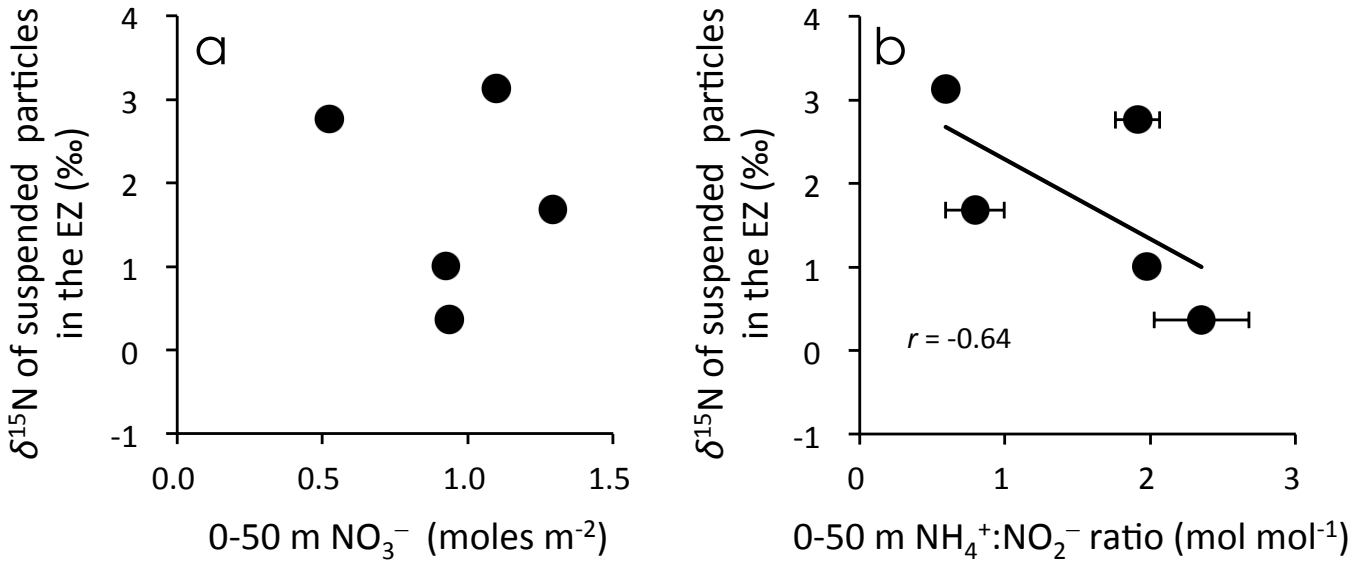

Figure 8 (Mino et al.)

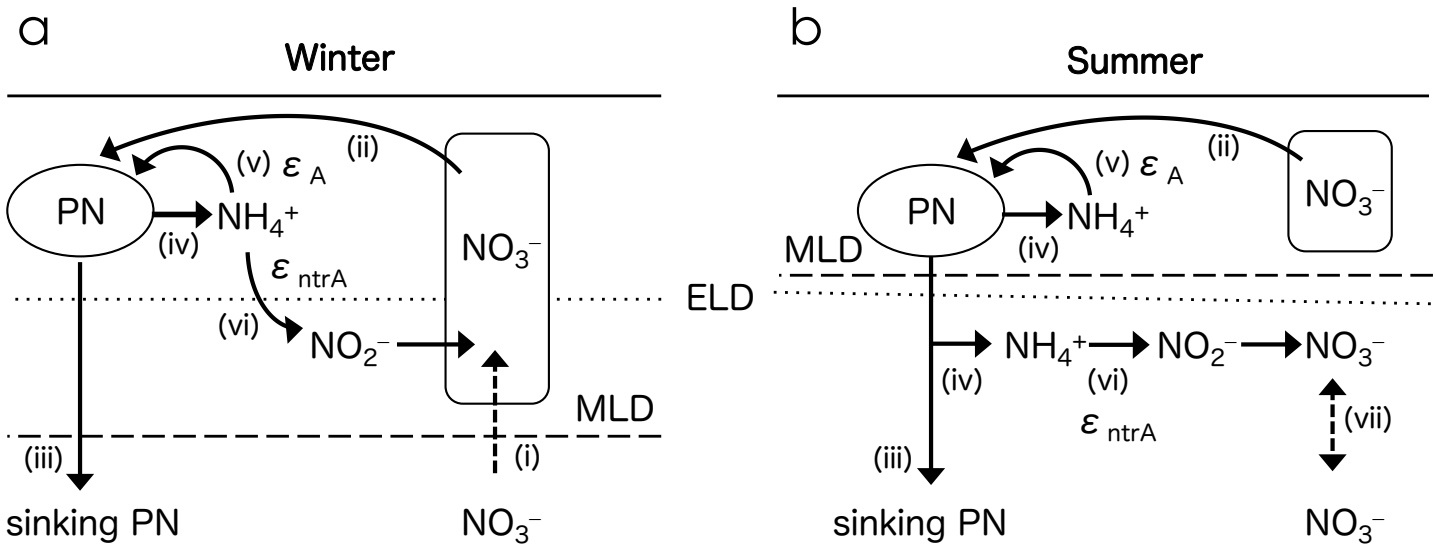

Figure 9 (Mino et al.)

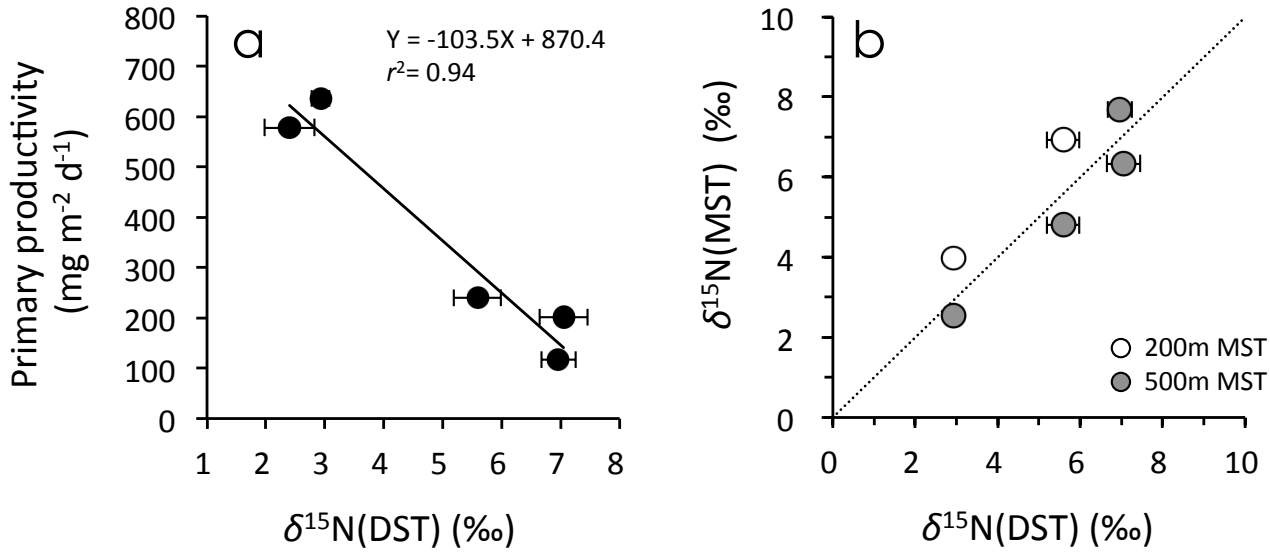

Figure 10 (Mino et al.)

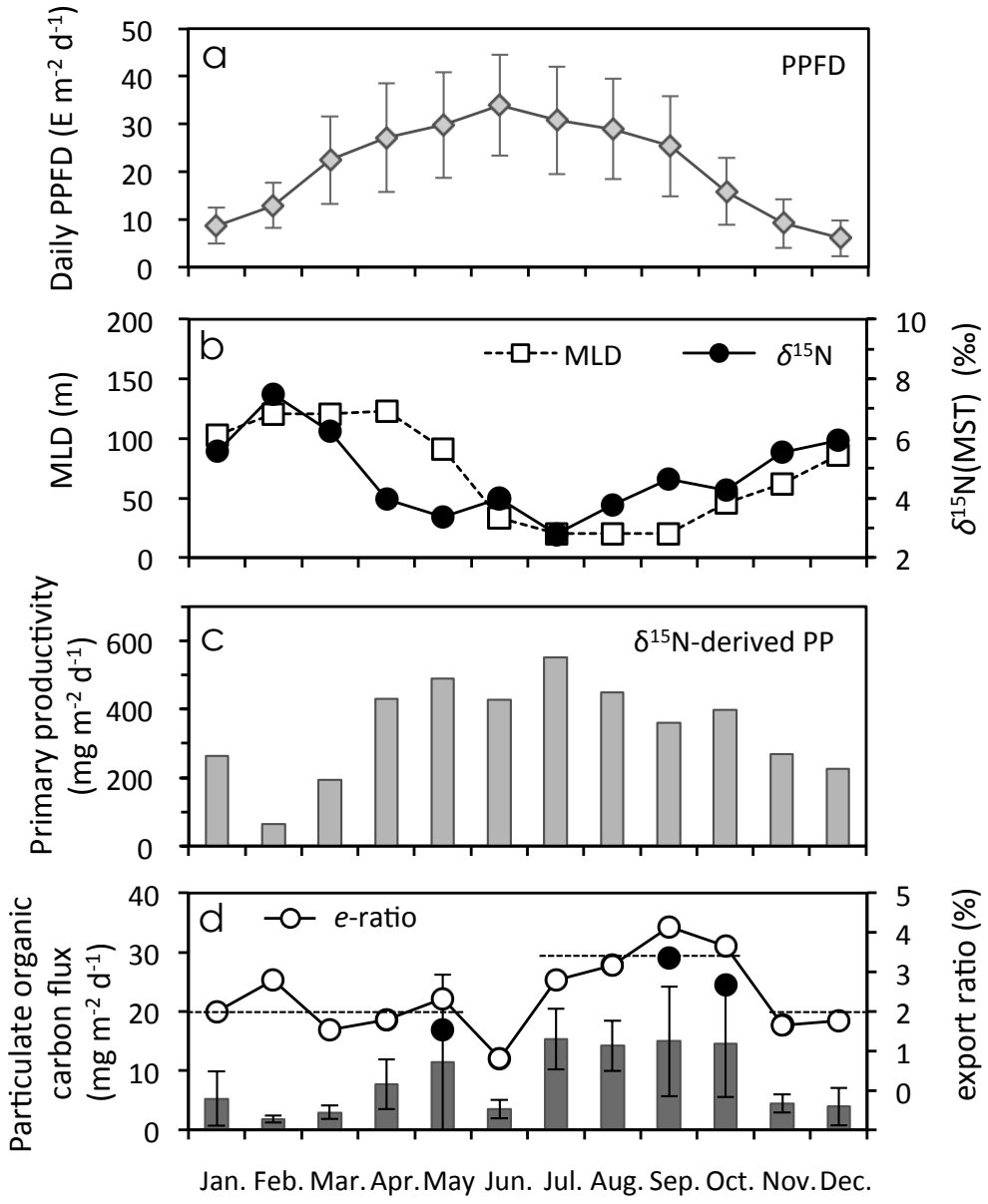

Table

Table 1 (Mino et al.)

variable	*r*	*n*	*p*
Total mass flux (mg m^{-2} d^{-1})	-0.52	55	<0.001
POC flux (mg m^{-2} d^{-1})	-0.50	55	<0.001
w(OC) (%)	0.28	55	0.037
w(opal) (%)	-0.32	55	0.018
R(opal:$CaCO_3$) (mol mol^{-1})	-0.44	55	<0.001
R(C:N) (mol mol^{-1})	-0.67	55	<0.001
Daily PPFD (E m^{-2} d^{-1})	-0.65	56	<0.001
SST (°C)	-0.38	56	0.007

Table 2 (Mino et al.)

Cruise	Date	δ^{15}N (‰) 0-50 m SUS, EZ	δ^{15}N (‰) 100-200 m SUS, deep	δ^{15}N (‰) 100-200 m DST	Δ^{15}N (‰) (DST – SUS, EZ)	*R*(C:N) (mole mole^{-1}) 0-50 m SUS, EZ	*R*(C:N) (mole mole^{-1}) 100-200 m SUS, deep	*R*(C:N) (mole mole^{-1}) 100-200 m DST	ΔR(C:N) (mole mole^{-1}) (DST – SUS, EZ)
MR10-06	October 2010	2.8	7.4	5.6	2.8	5.7	7.5	7.5	1.8
MR11-02	February 2011	3.1	6.5	7.0	3.8	6.0	6.6	7.2	1.2
MR11-03	April 2011	1.7	7.3	7.0	5.4	6.0	7.9	9.1 (7.3)[a]	3.2 (1.4)[b]
MR11-05	July 2011	0.4	5.3	2.9	2.6	6.0	7.0	8.1	2.1
MR12-02	June 2012	1.0	7.0	2.4	1.4	5.6	6.9	8.8	3.3
Ave. in 2010-2011		2.0	6.6	5.6	3.6	5.9	7.2	8.0 (7.5)[b]	2.1 (1.6)[b]
S.D in 2010-2011		1.2	0.9	1.9	1.3	0.1	0.5	0.8 (0.4)[b]	0.8 (0.4)[b]

Table 3 (Mino et al.)

variable	*r*	*n*	*p*
MLD	-0.42	12	0.20
MLD (except for June)	-0.68	11	0.030
w(OM)	0.67	12	0.025
w(opal)	-0.33	12	0.31
w($CaCO_3$)	0.31	12	0.35
R(C:N)	0.71	12	0.014